PLOS Water

RESEARCH ARTICLE

Removal of chromium(VI) from water utilizing a column loaded with H_3PO_4-activated *Areca catechu* waste

Prabin Basnet[1,2], **Kedar Nath Ghimire**[1], **Hari Paudyal**[1]*

1 Central Department of Chemistry, Tribhuvan University, Kirtipur, Kathmandu, Nepal, **2** Nepal Engineering College, affiliated to Pokhara University, Changunarayan, Bhaktapur, Nepal

* haripaudyal9@gmail.com

Check for updates

OPEN ACCESS

Citation: Basnet P, Ghimire KN, Paudyal H (2026) Removal of chromium(VI) from water utilizing a column loaded with H_3PO_4-activated *Areca catechu* waste. PLOS Water 5(4): e0000528. https://doi.org/10.1371/journal.pwat.0000528

Editor: Rakesh Kumar, Auburn University, UNITED STATES OF AMERICA

Received: June 8, 2025

Accepted: February 26, 2026

Published: April 2, 2026

Peer Review History: PLOS recognizes the benefits of transparency in the peer review process; therefore, we enable the publication of all of the content of peer review and author responses alongside final, published articles. The editorial history of this article is available here: https://doi.org/10.1371/journal.pwat.0000528

Copyright: © 2026 Basnet et al. This is an open access article distributed under the terms of the Creative Commons Attribution License, which permits unrestricted use, distribution,

Abstract

The current study evaluates the efficiency of a biosorbent produced from *Areca catechu* waste (ACW) for removing chromium(VI) from both synthetic and industrial water in a packed column system. ACW was initially activated with phosphoric acid (H_3PO_4) and thereafter carbonized to make phosphoric acid activated *Areca catechu* waste (PACW), where active sites were generated for the biosorption of chromium(VI) ions from the aqueous phase. Biosorption performance of PACW was measured under various operational conditions, where an equilibrium column capacity of 12.03 ± 0.08 mg/g was achieved at a continuous fluid flow rate of 2.33 mL/min. Furthermore, the experimental data were analyzed utilizing the linear and nonlinear forms of the Thomas, the Adams-Bohart, and the Yoon-Nelson models to evaluate the various column parameters. The column capacities from linear and nonlinear Thomas models were determined to be 11.74 ± 0.16 and 12.31 ± 0.16 mg/g, respectively. A study on industrial wastewater obtained from the carpet dyeing industry located in Jorpati, Kathmandu, Nepal, which contained 2.30 mg/L of chromium(VI), indicated that PACW could successfully reduce the chromium(VI) to 0.10 mg/L, meeting the water regulatory standard as specified by the World Health Organization. Therefore, the PACW investigated in this study demonstrates significant potential for the removal of trace amounts of chromium from contaminated water in a packed column setting.

1. Introduction

Water is one of the most vital components of human civilization, yet accessing unpolluted water has become a global worry in recent times [1]. Numerous pollutants and potentially hazardous substances can be found in water [2], among which chromium is the most dangerous [3]. The natural erosion of chromium-rich rocks and mineral deposits often contributes to chromium pollution, whereas human-induced chromium

and reproduction in any medium, provided the original author and source are credited.

Data availability statement: All data can be found in the manuscript and Supporting Information Files.

Funding: The author received no specific funding for this work.

Competing interests: The authors have declared that no competing interests exist.

pollution arises from various activities, particularly from metal polishing, leather tanning, electroplating, and chromate preparation [4].

The common oxidation states of chromium in aqueous solution are chromium(III) and chromium(VI). However, the chromium(VI) state is significantly more unsafe than the chromium(III) state due to its carcinogenic and toxic behavior [1,5,6]. Consequently, the WHO has recommended a limit of no more than 0.05 mg/L of chromium(VI) in drinking water [7]. There are various chromium(VI) removal methods that have been utilized over the decades, which include ion exchange [8], electrodeposition [9–11], chemical precipitation [12], and adsorption [13]. However, when dealing with wastewater containing trace concentrations, these techniques contain drawbacks such as incomplete removal, the necessity for advanced facilities, environmental challenges, and they are costly and inefficient [14,15]. Conversely, biosorption has emerged as a viable alternative for treating wastewater containing chromium(VI) ions from the aqueous phase [16].

Several plant-based materials [17–22] have been investigated over the past few decades, which have demonstrated potential in batch systems for removing chromium(VI) ions from water. These biomaterials contain phenols, carboxylic acids, and esters as polyfunctional groups; however, these functional groups are ineffective at biosorbing the metal ions due to their crystalline polymeric structure, hydrogen bonding, and hydrophobic nature [23]. Therefore, a certain methodology that may alter the surface of these biosorbents through either physical or chemical activation is necessary for improving their biosorption ability [24].

Among the surface activation techniques, pyrolysis is one of the widely used methods, which generates a carbonaceous compound from the biomaterial, in which the material is heated in an oxygen deficient atmosphere to start thermochemical breakdown, removing the inactive components from the material [25]. These synthesized carbonaceous compounds may contain an enhanced surface area and microporosity [26] besides the bioactive groups that can bind heavy metals such as chromium [27,28].

The biomaterials can also undergo multiple treatment techniques [29–31], but surface treatment with certain chemicals or chemical activation is found to be more effective [32].

In the chemical activation methods, generally, the biomass is treated with compounds like acids [33,34], bases [31], or salts [35]; however, the activation with acids is determined to be more effective since it has shown to create greater surface areas, microporosity, and functional groups [36], which is considered more favorable for the biosorption of various metals from the water [37].

Quite a few researchers have evaluated the chromium(VI) removal efficiency of various lignocellulosic materials obtained from the biological waste in the fixed bed column [38–53]. Some researchers have previously utilized multiple parts of the *A. catechu* plant [54–59]. However, to the best of our knowledge, *Areca catechu* waste, specially its sheath, has not been explored as a biosorbent until now, which offers a huge possibility in the removal of metals like chromium from water. *A. catechu* waste highly comprises cellulose (57.3%), hemicellulose (13.3%), and lignin (22%) [60],

which have different polyfunctional groups that, during the heat activation with H_3PO_4, can potentially undergo functional group and surface changes, providing active sites favorable for the efficient biosorption of chromium(VI). Moreover, *A. catechu* has been grown in very high amounts in Nepal. During the refining of *A. catechu*, a large volume of garbage is produced, which is normally dumped or biodegraded. As a result, the management of such a cast-off material to manufacture useful substances to remove toxic elements offers a viable alternative for *A. catechu* cultivators in elevating their financial position and also for the fineness of the ecosystem. Therefore, the authors intended to synthesize biosorbent from the readily available biological waste material by activating the *A. catechu* sheath with the acid, in which the process does not produce any secondary sludge and does not involve any chemicals other than the acid itself. Consequently, the goal of this research was to create a possibly low-cost, efficient, and biodegradable polymer capable of removing hazardous metals like chromium from the aqueous phase.

In the previous study, a biosorbent was developed by charring *A. catechu* waste (ACW) with concentrated H_2SO_4 to synthesize charred betel nut waste (CBNW) [24]. Although the CBNW successfully removed chromium(VI) from aqueous medium, there was a partial dissolution of this biosorbent in alkaline environments that led to the degradation of the available active sites for the biosorption of chromium(VI) ions. Thus, it was intended to form a biosorbent from the same biomass that could have greater biosorption efficiency and robustness than the biosorbent synthesized before. Moreover, the prior investigations have shown that the treatment of the biomass with phosphoric acid can change the surface structure of the material, which can highly improve its biosorption abilities [51,61].

Hence, in the previous investigation, the authors prepared a biosorbent from the ACW after its treatment with ortho phosphoric acid, followed by its thermal activation to develop phosphoric acid activated *A. catechu* waste (PACW), which was used to examine its chromium(VI) removal efficacy in batch mode [62]. From the investigation, it was discovered that the chromium(VI) uptake efficacy of PACW was substantially higher than that of CBNW [24], which was due to the increase in roughness or porosity on the PACW surface and the formation of an open-ring structure. Such a structure and functional groups are more suitable for the active participation in the biosorptive removal of chromium(VI) ions from the aqueous phase.

Nevertheless, the batch equilibrium experiments are not always transferable to a dynamically packed fixed bed column, where equilibrium is hardly reached owing to inadequate time of contact [63]. Hence, to operate a full scale biosorption system, a dynamically packed column is thought to be more appropriate for the removal of pollutants from wastewater. As a result, the authors aimed to continue the work with PACW to investigate the feasibility of water polluted with chromium(VI) ions in a fixed bed setting.

In this investigation, the surface modification of PACW was established by several spectroscopic methods, along with the Brunauer-Emmett-Teller (BET) and zeta potential analyzer. The effectiveness of the chromium(VI) removal was subsequently evaluated using simulated as well as industrially polluted water. The effects of various operating parameters like pH, fluid flow rate, influent chromium(VI) concentration, and bed height were systematically examined, whereas the design parameters were determined by dynamic modeling using the Thomas, the Adams-Bohart, the Yoon-Nelson, and the Bed Depth Service Time (BDST) model.

2. Materials and methods

2.1. Chemicals and reagents

All the chemicals and reagents used in this study were either AR (analytical reagent) or ACS grade and were not purified further before use. The sulphuric acid (H_2SO_4, 98%), potassium dichromate ($K_2Cr_2O_7$, > 99%), orthophosphoric acid (H_3PO_4, 85%), sodium hydroxide (NaOH, > 99%), sodium bicarbonate ($NaHCO_3$, > 99%), and buffer solutions were analytical grade chemicals and supplied from Fisher Scientific Pvt. Ltd., India. Analytical graded hydrochloric acid (HCl, 35%) solution was provided by Merck Chemicals Company Pvt. Ltd, India, whereas diphenyl carbazide ($C_{13}H_{14}N_4O$, 99%) was provided by Loba Chemical Pvt. Ltd, India. A stock solution of chromium(VI) was prepared by dissolving 2.82 grams of

$K_2Cr_2O_7$ in one liter of double distilled water to get a 1000 mg/L of it. The working solutions were prepared from the stock solution by diluting the stock solution at the time of the experiment. Dilute solutions of HCl and NaOH (0.1M each) were used to adjust the pH of the solution.

The laboratory work was conducted at the research laboratory of the Central Department of Chemistry, Institute of Science and Technology, Tribhuvan University, Kirtipur, Kathmandu, Nepal, under the supervision of Assistant Professor Dr. Hari Paudyal from the same department.

2.2. Preparation of biosorbent from *A. catechu* waste

In Nepal, ripe and mature nuts of *A. catechu* are generally harvested once a year in the spring season (April-May) and are collected, processed, and stored by various *A. catechu* processing companies. The unhusked ripe seeds (Mangala variety), which were naturally covered with the sheath, were collected directly from the *A. catechu* cultivator from Arjundhara, Jhapa, Nepal, after which the seeds were husked or peeled. The waste product thus obtained, which is abbreviated as ACW here, was repeatedly cleaned with water and oven-dried, after which it was finely crushed and sieved to obtain particles with a size smaller than 150 μm. After this, chemical modification of ACW was conducted by following the methods as mentioned by Shrestha [32] with a slight modification, which is described as follows: 25 grams of ACW was treated with H_3PO_4 in a ratio of 1:1 (weight/weight). It was then allowed to settle in a crucible for a complete day. Afterward, the product was placed into a silicon boat and then heated using a tube furnace for about 4 hours at 400 °C with a constant supply of N_2 (100 mL/min) gas. During the process, the material was carbonized, where there was a removal of volatile compounds from the material. To remove excess amounts or traces of phosphoric acid that could be present in the residue, the carbonized product was immersed in a 1% $NaHCO_3$ solution to neutralize the excess acid. After getting a neutral pH, the prepared material was cleansed with distilled water and then oven dried. The final product thus obtained, named as phosphoric acid activated *A. catechu* waste (PACW), was finally ground into a fine powder. This product was employed in a chromium(VI) biosorption process in a fixed column bed in continuous mode.

2.3. Characterization of biosorbents

The diffraction patterns of the dried powder of raw ACW and PACW were recorded using Cu K_α radiation of wavelength 0.15418 nm at 1 degree per minute of scanning rate from 2θ angles in between 5° and 80° by utilizing an X-ray diffractometer (Rigaku Co., Japan). The FTIR (Fourier Transform Infrared Spectra) of the biosorbents before and after the biosorption were collected at a resolution of 2 cm^{-1} by using the spectrometer (SHIMADZU, Kyoto, Japan) in between 4000 and 500 cm^{-1}. Also, the surface morphology of the biosorbents before and after chromium(VI) treatment was measured by utilizing an SEM-EDX analyzer (JEOL JSM-6400F) at the 10 kV acceleration voltage. The zeta potential of the biosorbent at various pH levels was recorded to investigate the biosorbent surface charge by using a zeta potential analyzer (HORIBA Scientific SZ-100).

Moreover, the Brunauer-Emmett-Teller (BET) surface area, as well as pore volumes, pore size distribution, micro-meso pore area, and average pore diameter, were assessed using a BET analyzer employing a Quantachrome instrument (Quantachrome NovaWin ©1994–2018, v11.05). The surface area was evaluated through N_2 gas sorption-desorption within a relative pressure between 0.0068 and 0.9912 Pascal at 77.35 K of temperature. The BET equation is generally expressed as follows [64]:

$$\frac{1}{V\left[\frac{P_o}{P}-1\right]} = \frac{C-1}{V_m C}\left(\frac{P}{P_o}\right) + \frac{1}{V_m C} \tag{1}$$

Where V represents the volume of the gas which is biosorbed, V_m denotes the volume of N_2 gas biosorbed at standard temperature and pressure (STP) to achieve monolayer sorption on the material, P_o and P indicate the saturated as well

as partial vapor pressure of the biosorbed gas in equilibrium, respectively with the surface at 77.3 K of temperature. Also, C represents a constant associated with the enthalpy of the gas which is undergoing the biosorption, and P/P_o represents the relative pressure.

2.4. Dynamic biosorption of chromium(VI) in packed column setting

The dynamic biosorption test was conducted in a glass column with 0.8 cm of inner diameter and 20 cm of total height. PACW was soaked in deionized water at an optimum pH of 1 for 12 hours before packing. The soaked PACW was packed according to the procedure described in Paudyal et al as follows [65]: At first, glass beads were inserted (3 cm) into the column, then the column was packed with a cotton layer (2 cm) and then with the wetted PACW with no air bubbles. After the homogenous packing of PACW, the biosorbent bed was covered by a cotton layer (2 cm) followed by glass beads (3 cm) to prevent the floating of the PACW bed under the continuous flow of influent solution. The pH of the influent chromium(VI) solution was adjusted by supplying a small amount of 0.5 M hydrochloric acid or sodium hydroxide solution. A continuous flow of chromium(VI) solution at a predetermined fluid flow rate was maintained with the use of a peristaltic pump (Iwaki model, 100N). Afterward, the influential parameters (pH, chromium(VI) concentration, bed height, and fluid flow rate) were evaluated as depicted in the flowsheet diagram (Fig 1).

After the column treatment, the discharged samples (the effluent) were gathered from the exit at predetermined time gaps. The chromium(VI) ions in the solution pre- and post-column treatment were evaluated by developing a color through the 1, 5-diphenylcarbazide method as described by Demiral et al [66] using the Beer-Lambert law [67]. The column was run until the optimum capacity of the biosorbent was reached, which was characterized by the observation of the same

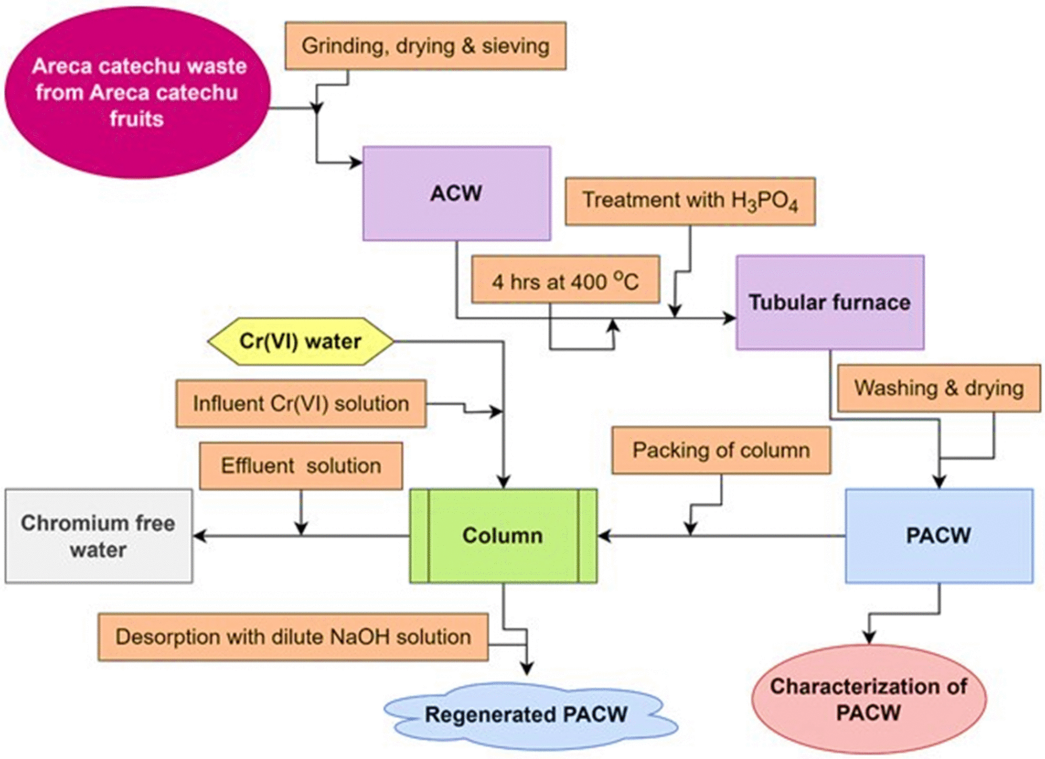


Fig 1. Flowsheet diagram showing the synthesis of biosorbent, characterization & biosorption of chromium(VI) ions.

https://doi.org/10.1371/journal.pwat.0000528.g001

concentration of chromium(VI) in influent as well as effluent solutions; this condition is known as column saturation. After the saturation, various column parameters such as mass transfer zone (Δt), column capacity, and effective volume (V_{eff}) were determined according to the following relations [66,68]:

$$(\Delta t) = t_e - t_b \tag{2}$$

$$q_{total} = \frac{FA}{1000} = \frac{F}{1000}\int_{t=0}^{t=total} (C_i - C_e)\, dt \tag{3}$$

$$V_{eff} = F \times t_{total} \tag{4}$$

$$q_{equ} = q_{total/M} \tag{5}$$

Where t_e is the exhaustion time, whereas t_b is the breakthrough time, F is the fluid flow rate of influent solution (mL/min), and A (cm^2) is the area under the breakthrough diagram. Also, V_{eff} represents the effective volume treated, which is equal to the product of total treated time (t_{total}) and fluid flow rate (F), M is the dry weight of PACW (g) packed in a column, and q_{equ} (mg/g) is the equilibrium concentration of chromium(VI) biosorbed by the column per unit mass of PACW, which was evaluated by dividing q_{total} (total amount of chromium(VI) biosorbed onto the biosorbent bed in mg) by the mass of the PACW as depicted by the equation(5) [40].

2.5. Statistical analysis

It is always necessary to identify the validity, precision, and accuracy of the evaluated data, for which the research outcome should always be checked by using valid and well adopted statistical models. In the present context, various parameters such as the χ2 test, RSS, the residual sum of squares, TSS, the total sum of squares, and R^2, the coefficient of determination, were utilized. The mathematical expressions (equations 6–10) for these parameters are given below:

$$RSS = \sum_{i=1}^{n} (q_{i,equ} - q_{i,o})^2 \tag{6}$$

$$TSS = \sum_{i=1}^{n} (q_{i,equ} - q_{equ,average})^2 \tag{7}$$

$$R^2 = 1 - \frac{RSS}{TSS} \tag{8}$$

Alternatively,

$$R^2 = 1 - \frac{\sum_{i=1}^{n} (q_{i,equ} - q_{i,o})^2}{\sum_{i=1}^{n} (q_{i,equ} - \overline{q}_{i,equ})^2} \tag{9}$$

$$\chi^2 = \sum_{i=1}^{n} \frac{\left(q_{i,\mathrm{equ}} - q_{i,\mathrm{o}}\right)^2}{q_{i,\mathrm{o}}} \tag{10}$$

Where i is the data number, $q_{i,equ}$ is the experimentally observed biosorption capacity, $\overline{q}_{i,equ}$ is the mean of the experimentally observed biosorption capacity, and $q_{i,o}$ is the calculated amount of biosorbed ions from the most fitted models in mg/g.

3. Results and discussion

3.1. Characterization of biosorbents

To validate the surface variations taking place before and after the chemical treatment of the biomaterial, it is generally essential to employ advanced characterization instruments, as demonstrated in various studies conducted previously [69]. In this study, the authors utilized characterization tools including XRD to assess the roughness of the material's surface, FTIR to identify the active functional groups involved in the biosorption process, SEM and EDX to analyze the elemental compositions, and BET to determine the surface porosity.

3.1.1. Surface area analysis. The measurement of the surface area of the material is crucial in the biosorption process, necessitating its examination [70]. As per the International Union of Pure and Applied Chemistry (IUPAC), the materials are categorized into three groups: i) microporous with the pore diameter less than 2 nm, ii) mesoporous with the pore diameter from 2 to 50 nm, and iii) macroporous with the pore diameter greater than 50 nm [66,71]. Supplementary figure 1 (S1 Fig) presents the results derived from the BET analysis using the Barrett-Joyner-Halenda (BJH) and Dollimore-Heal (DH) methods for the pore size distribution. The corresponding major values and the overall data are listed in S1 Table and S1 Data, respectively.

The figure shows that the biosorption-desorption plot (S1A Fig) is a type II isotherm [72]. Also, it can be observed that biosorption is faster at the lower value of relative pressure (0.0068-0.0585 Pa), which is attributed to the easily available surface and direct contact of adsorbate and biosorbent, leading to a monolayer surface coverage and attaining a faster equilibrium. Moreover, in the figure, a surface area ranging from 117.99 to 138.25 m^2/g has been attained at a pore size of 6.91 to 28.87 nm (S1B Fig) and total pore volume (VT) = 0.169 cm^3/g has been achieved at the pore size of less than 28.87 nm (S1C Fig) showing that the material is mostly mesoporous. The cumulative volume distribution curve (S1D Fig) and surface area distribution curve (S1E Fig) reveal significant peaks within the pore width of 1.80 to 9.83 nm, demonstrating the existence of both micro- and mesopores in the biosorbent. Also in the figure, the mesopore volume is 0.145 cm^3/g, which is 85.79% of the total volume covered by the pores. In contrast, only 14.20% of the pores are covered by the micropores. This indicated that the chemical treatment of the ACW successfully created micropores in a minor amount and mesopores in a major amount. Furthermore, as can be seen in the isotherm figure (S1A Fig), as the pressure increases, the biosorption increases drastically without attaining equilibrium. This often happens if there is a presence of mesopores of greater surface area, where faster surface coverage is not possible, and also, there is always a chance of multilayered biosorption of the adsorbate (N_2) if there is a larger pore size and surface area.

3.1.2. Surface morphology and elemental analysis. The surface morphology of the biosorbent is considered to change after chromium(VI) biosorption, so scanning electron micrographs of the ACW and PACW pre and post biosorption were collected as depicted in Fig 2 [73,74]. As can be observed in Fig 2A, the SEM image of ACW possesses some patches and irregular surface morphology, whereas in the SEM image of PACW (Fig 2B), the surface appears relatively rough, which is presumed to be much more favorable for biosorption of the targeted metal ions.

Interestingly, in the case of chromium(VI) treated PACW (Fig 2C), the majority of channels and pores are found to be filled, which is attributed to the effective biosorption of chromium(VI) on the PACW. A similar observation was noticed by Rai et al using acid treated pomegranate peel [75]. Hence, these findings strongly supported the modifications in the

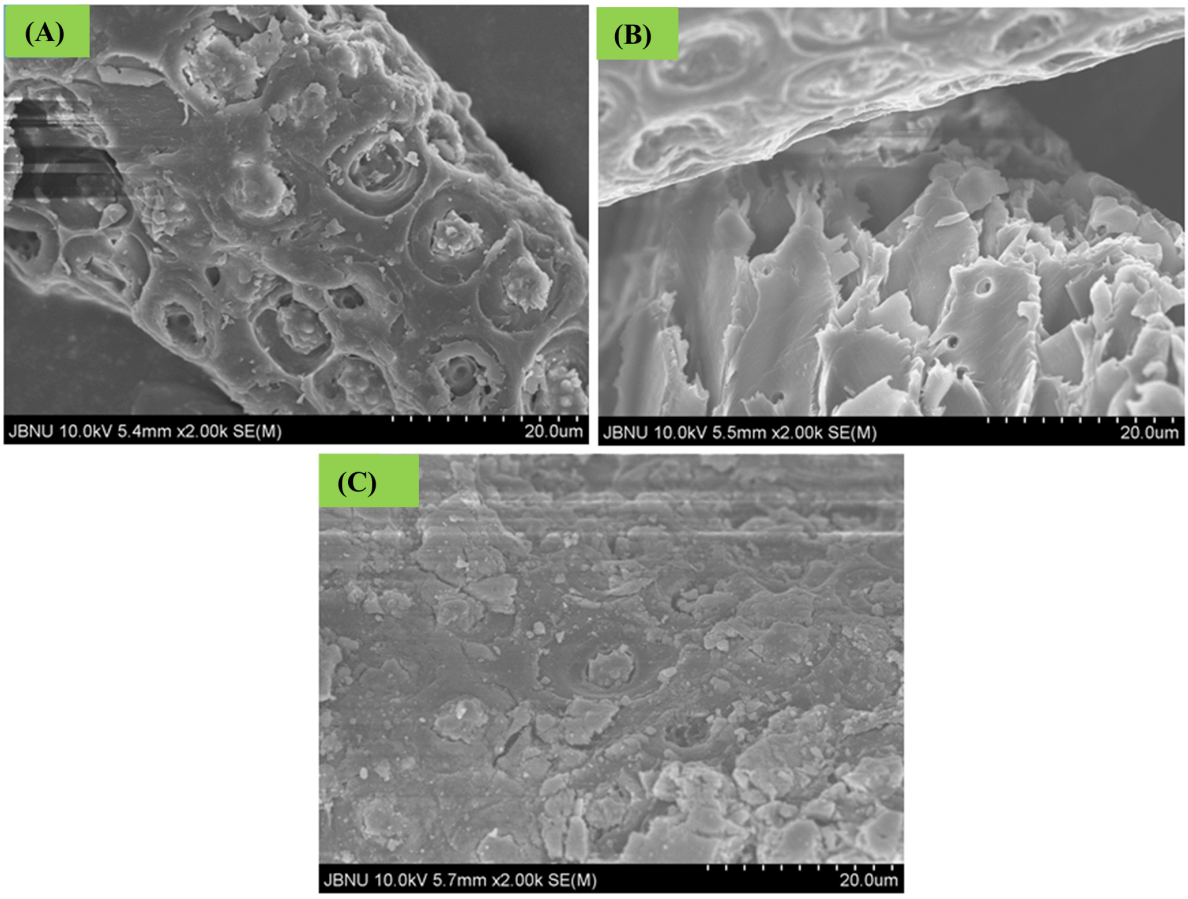


Fig 2. SEM images of (A) native ACW, (B) PACW, and (C) PACW after chromium(VI) biosorption at 2000 times (2.00 k) magnification.

https://doi.org/10.1371/journal.pwat.0000528.g002

surface of *A. catechu* waste during the treatment of the material with the acid and the chromium(VI) solution, which was further verified by elemental analysis using EDX spectroscopy.

Fig 3 shows the elemental distribution and mapping of individual elements with different colors, together with EDX spectra. The distribution of various elements on the surface of PACW pre (Fig 3A) and post chromium(VI)-PACW contact (Fig 3B) in the packed column bed has been depicted by various colors inside the figures. The figure shows the heterogeneous distribution of elements on the surface of the PACW, as well as the chromium(VI)-treated PACW.

In the color mapping image (Fig 3A), it can be seen that carbon (C, red) and oxygen (O, light green) are major elements, whereas silicon (Si, blue) and phosphorus (P, orange) are in trace amounts. However, in Fig 3B, an additional element, chromium (Cr, light orange), can be observed on the surface, which strongly suggests the biosorption of the chromium(VI) ion onto the PACW. Moreover, in the energy distribution graph (Fig 3A), PACW shows intense peaks of C and O at 0.28 and 0.52 keV of binding energies, in addition to the minor peaks corresponding to Si and P at binding energies of 1.73 and 2.01 keV, respectively. This indicated that carbon and oxygen were present as the major elements in PACW, which is attributed to the various polysaccharides of *A. catechu* waste, including cellulose, hemicellulose, lignin, and protein. On the other hand, in Fig 3B, an entirely new peak equivalent to elemental chromium(Cr) can be seen at a binding energy of 5.40 keV. This finally confirmed that PACW effectively biosorbed chromium(VI) ions after the PACW-Cr(VI) contact.

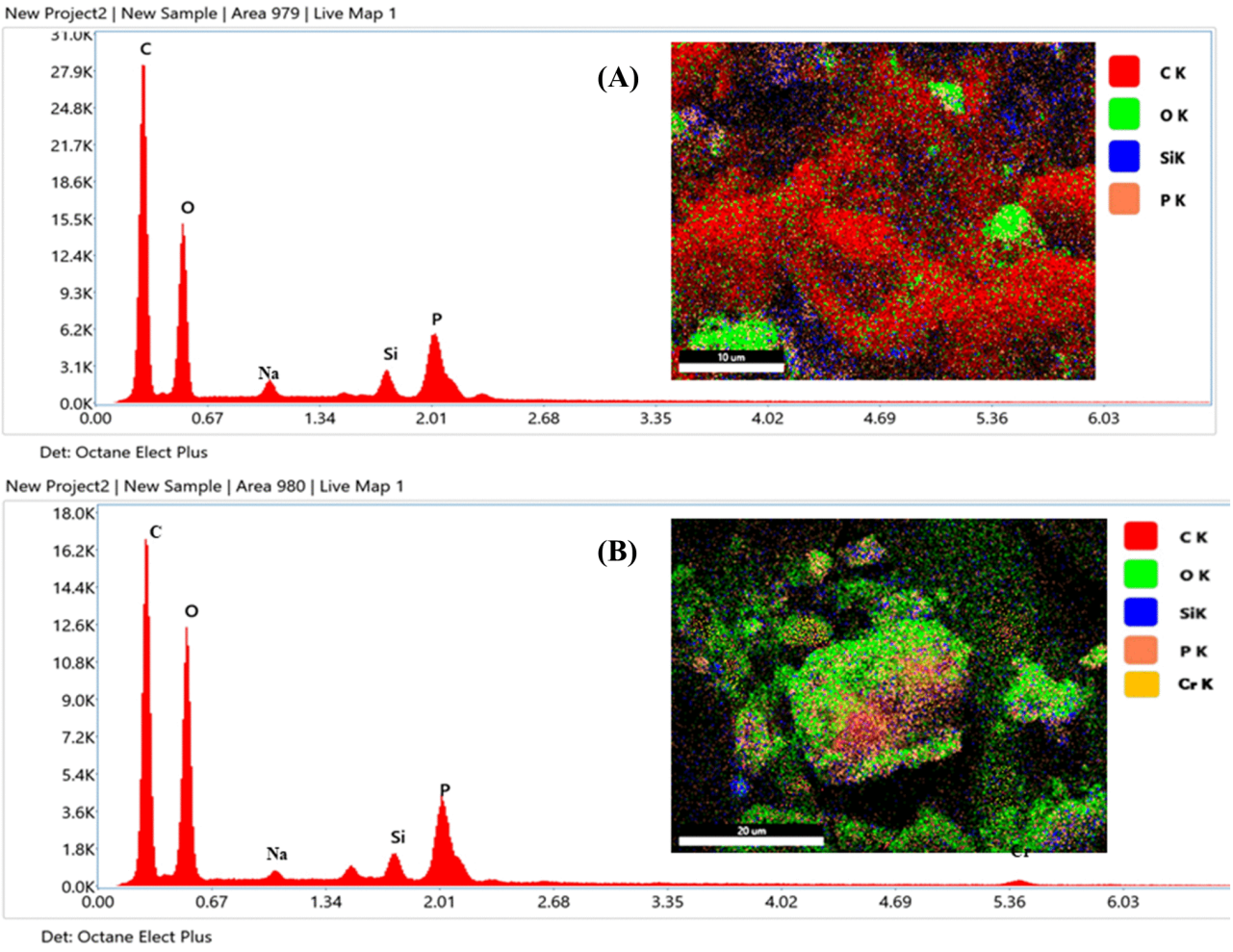


Fig 3. EDX spectra with the elemental distribution of PACW (A) before and (B) after chromium(VI) biosorption.

https://doi.org/10.1371/journal.pwat.0000528.g003

3.1.3. Functional group changes and crystalline property. The FTIR spectra (S2 Data) of the ACW and PACW (Fig 4A) were analyzed to determine any changes that might have occurred as a result of the phosphoric acid treatment, which is thought to be beneficial in the biosorption of chromium(VI). The ACW, which initially revealed a broad peak at 3516.40 cm^{-1} due to the OH group, shifted slightly to 3402.43 cm^{-1} at PACW. Also, it was found that the peaks observed at 2075.53, 1572.19, and 1853.59 cm^{-1} in the ACW disappeared in PACW, which is directly associated with the structural changes of these groups due to the phosphoric acid treatment. Besides, a prominent peak at 1654.92 cm^{-1} demonstrated the presence of C = O, a new functional group in the PACW [76], suggesting that the cellulose ring opening of the ACW had occurred during its treatment with phosphoric acid, as demonstrated in S1 Scheme, step 1. Moreover, there were new peaks at 1381.03 and 1251.80 cm^{-1} attributed to OH and C-O groups, respectively, which suggested that the surface of the ACW was significantly changed after its treatment with the acid. Also, after the treatment of the PACW bed with the chromium(VI) solution, there was a change in the peak intensities, which signified the biosorption of chromium(VI), as shown in S1 Scheme, step 3. A similar occurrence was recorded by Pant et al and Rai et al when they treated *Areca catechu* nut leaf sheath and pomegranate peel individually with H_2SO_4 [75,77].

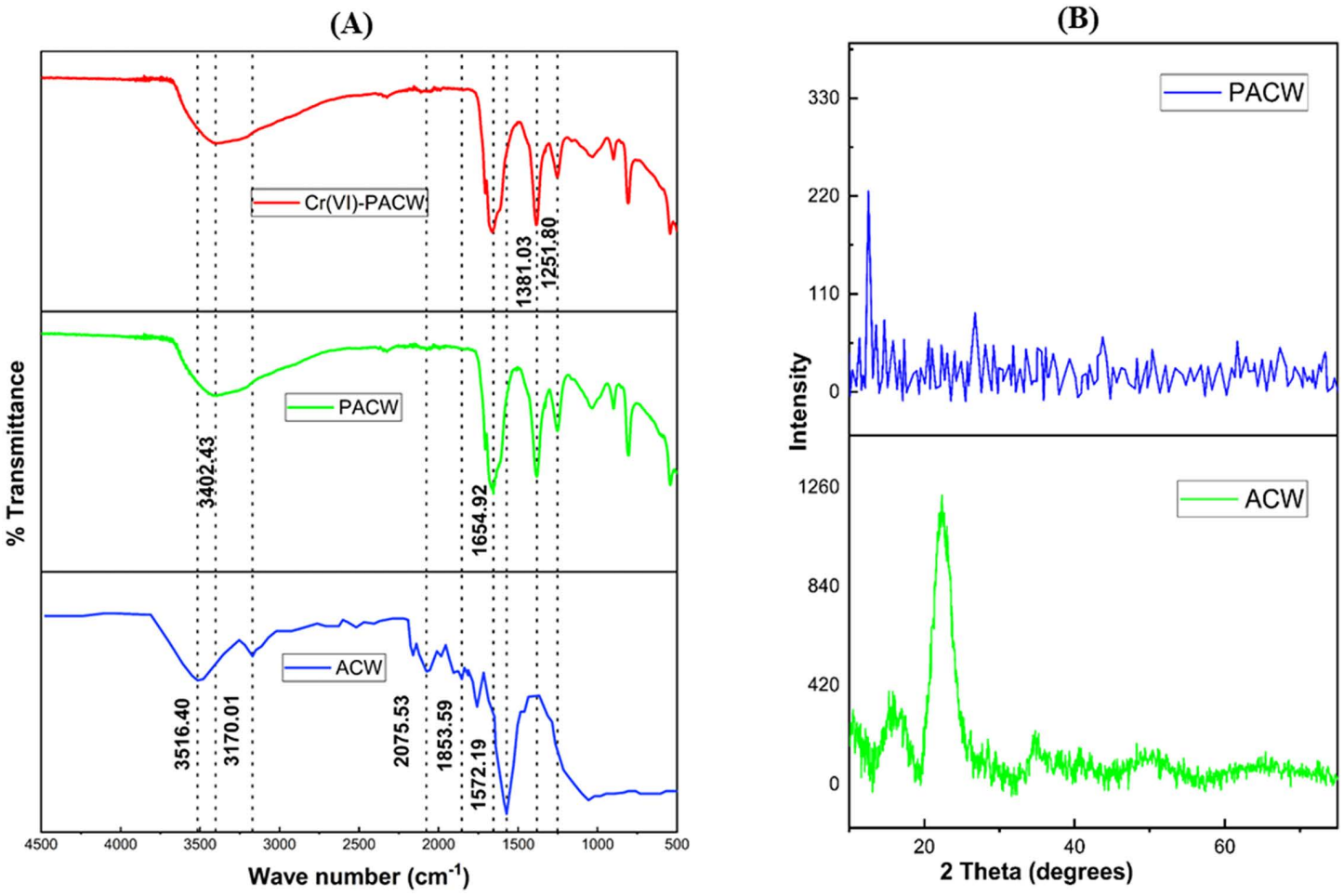


Fig 4. (A) FTIR spectra of ACW, PACW, and PACW after the treatment with chromium(VI) ions and (B) XRD pattern of ACW and PACW showing the change of crystalline property during chemical modification.

https://doi.org/10.1371/journal.pwat.0000528.g004

It has been found in prior studies that the biosorbent with the amorphous surface favors biosorbing chromium(VI) from the water more than the crystalline surface [24]. This is because, in the crystalline form, the polyfunctional groups such as OH and COOH are tightly packed and exposed less to the chromium(VI) ion, due to which they are ineffective. Generally, the crystallinity in the material is indicated by the peak intensity in the XRD analysis. Sharp, clean, and intense peaks in the XRD indicate a crystalline nature, while wide and rough peaks represent the amorphous nature of the material. During the analysis, peaks were examined after the XRD data were corrected for baseline using OriginLab 18-Pro software to identify the smooth peaks. As can be noticed in the figure (Fig 4B), ACW shows a minor peak at 2Θ around 34.85 degrees and a strong peak at 15.52 and 22.33 degrees, which correspond to the crystallinity of the cellulose. However, in the PACW, the peaks, which correspond to the crystallinity, completely disappear at all three places. In place of those peaks, broader peaks can be seen at 5.63 and between 11.89 and 16.37 degrees of 2Θ. This finally demonstrated that the acid treatment of the ACW changed the crystallinity of the ACW's cellulose into an amorphous state, which is generally considered suitable for the binding of chromium(VI) ions onto the material.

3.2. Biosorption of chromium(VI) in a column of a fixed bed

3.2.1. Influence of pH and mechanism of chromium(VI) biosorption. The pH of the aqueous phase has been considered one of the major controlling factors for the surface charge of the biosorbent and chromium(VI) biosorption. Moreover, it is always crucial to examine the pH where the surface of the biosorbent has zero charge, since material with positively charged surfaces has been found to improve the biosorption of oxonions such as chromium(VI) tremendously. In this test, a zeta potential analyzer was used, which helps to evaluate the neutral point at the surface of PACW at the optimal pH (pHpzc). Supplementary figure 2 (S2 Fig) demonstrates how PACW's surface charge was impacted by the pH of the aqueous phase. Here, the pHpzc was evaluated to be 5.4. Below this pH, the PACW surface was found to have positive charges. This phenomenon is attributed to the attachment of H^+ ions with the hydroxyl groups present in the PACW (S1 Scheme, step 2). Fig 5A, which is called a breakthrough curve or breakthrough diagram, illustrates the relationship between the ratio of outgoing and incoming concentration (C_e/C_i) with treated time at different pHs.

The results showed that t_b dropped from 180 min to 120 min while moving from pH 1–4 during the biosorption (Table 1).

Here, C_i represents the influent concentration of chromium(VI) ions (mg/L), t_{total} denotes the total time to achieve the equilibrium (min), V_{eff} represents the total volume treated (mL), t_b represents the breakthrough time (min), t_e represents the time of exhaustion (min), q_{total} represents the total quantity of chromium(VI) biosorption (mg), q_{equ} denotes the equilibrium biosorption capacity of PACW (mg/g), Z represents the height of the bed (cm), F represents the fluid flow rate (mL/min) and Δt represents the zone of mass transfer (min).

The greatest t_b was found at pH 1, and maximum biosorption of chromium(VI) occurred at this pH inside the packed column. Actually, chromium(VI) mostly occurs in water as the $HCrO_4^-$ anion at this pH (1–4) value [75]. Also, PACW provided suitable complexing sites for the binding of $HCrO_4^-$ ions as depicted in S1 Scheme with a greater specific surface area, which significantly enhanced the chromium(VI) biosorption. The equilibrium column capacities for chromium(VI) ion at pH 1, 2, and 4 were determined to be $12.03 \pm 8.0 \times 10^{-2}$, $5.84 \pm 3.5 \times 10^{-2}$, and $4.36 \pm 3.5 \times 10^{-2}$ mg/g, respectively. The increased biosorption capacity at pH 1 was due to the strongly positive surface of the PACW, which led to a strong attraction between the PACW surface and the $HCrO_4^-$ ions. Finally, this resulted in a complexation reaction as depicted in S1 Scheme, step 3, with the release of water molecules. On the other hand, as the pH was raised, the PACW surface became less positive, demonstrating the deprotonation of the hydroxyl group, which eventually made the biosorption of chromium(VI) anions unfavorable, hence resulting in the decrease in the biosorption capacity.

3.2.2. Impact of fluid flow rate of chromium(VI) solution. The influence of the speed or rate of the influent chromium(VI) solution on the biosorption behavior of the PACW bed was examined at fluid flow rates of 2.33 and 3.33 mL/min, keeping pH (pH = 1), bed depth or height (0.5 cm), and chromium(VI) concentration (1.02 mg/L) constant at room temperature, and the data obtained are introduced in Fig 6A.

The result indicated that when the speed of fluid was increased from 2.33 to 3.33 mL/min, the breakthrough time (t_b) dropped from 180 to 60 minutes, and the chromium(VI) quantity biosorbed by the column reduced from $12.03 \pm 8.0 \times 10^{-2}$ to $10.13 \pm 9.5 \times 10^{-2}$ mg/g (Table 1). Here, the reduced fluid flow rate increased the time of exposure between chromium(VI) ions and the PACW surface. However, at a greater fluid flow rate, the chromium(VI) ions, which were entering the column, could not receive adequate time to interact with the surface of the PACW, which led to a faster breakthrough and consequently resulted in reduced column capacity [15,78]. On the other hand, the t_e decreased from 900 to 660 min after increasing the fluid flow rate, which was because of the rise in the total chromium(VI) ions available for biosorption reaction, due to which the saturation was achieved faster [79].

3.2.3. Impact of bed height for chromium(VI) biosorption. Fig 7A displays breakthrough plots for chromium(VI) ions on the PACW at various bed depths/or heights. The PACW mass packed in a column for bed heights of 0.25, 0.50, and 0.75 cm were 50, 100, and 150 mg, respectively. As expected, it was found that the treated volume (V_{eff}) of chromium(VI) solution, Δt, $t_{b,}$ and t_e were increased with increasing the bed height. As the depth of the PACW bed was raised, the equilibrium column capacity decreased, which was because the channeling effect was more prevalent in the case of the column at a greater

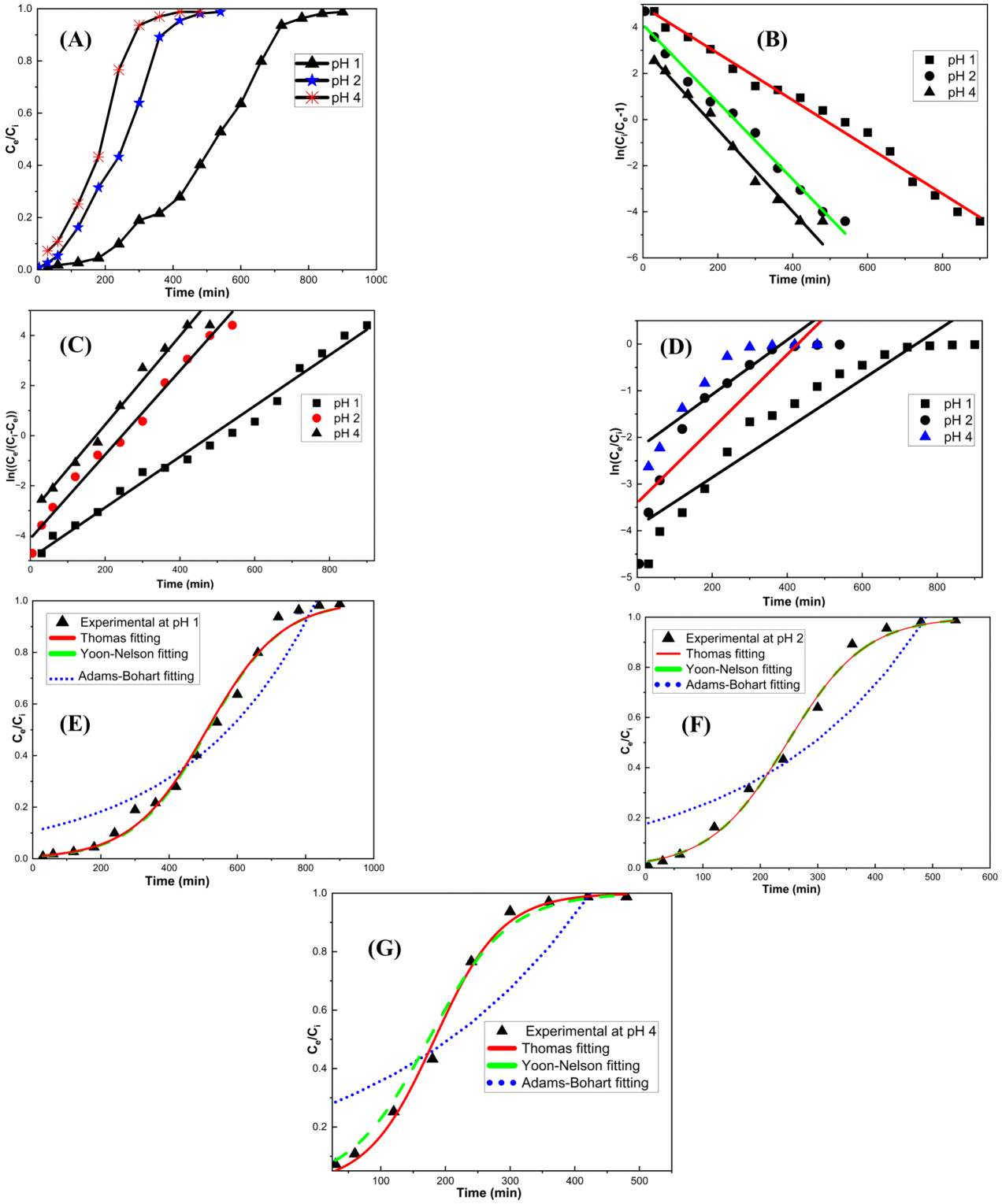


Fig 5. The breakthrough profiles of chromium(VI) ions at various pHs. (A) breakthrough plot of experimental data, (B) Thomas linear plot, (C) Yoon-Nelson linear plot, (D) Adams-Bohart linear plot and, (E, F & G) nonlinear plots of Thomas as well as Yoon-Nelson and Adams-Bohart expressions along with the experimental data (**condition**: fluid flow rate = 2.33 mL/min, influent concentration of chromium(VI) ions = 1.02 mg/L, pH = 1–4, and depth of the bed = 0.5 cm).

https://doi.org/10.1371/journal.pwat.0000528.g005

Table 1. Estimated column parameters for the biosorption of chromium(VI) in a column filled with PACW (S3 Data).

Para meters	F (mL/min)	Z (cm)	M (mg)	pH	C_i (mg/L)	t_b (min)	t_e (min)	Δt (min)	V_{eff} (mL)	t_{total} (min)	q_{total} (mg) X 10^{-3}	q_{equ} (mg/g) X 10^{-2}
Bed depth (Z)	2.33	0.25	50	1	1.02	60	420	360	1118.40	480	0.44 ± 4.3	8.90 ± 8.3
	2.33	0.50	100	1	1.02	180	900	720	2097.00	900	1.20 ± 7.5	12.03 ± 8.0
	2.33	0.75	150	1	1.02	240	960	720	2516.40	1080	1.45 ± 14.1	9.69 ± 9.0
Fluid flow rate (F)	2.33	0.50	100	1	1.02	180	900	720	2097.00	900	1.20 ± 7.5	12.03 ± 8.0
	3.33	0.50	100	1	1.02	60	660	600	2397.60	720	1.01 ± 9.5	10.13 ± 9.5
pH	2.33	0.50	100	1	1.02	180	900	720	2097.00	900	1.20 ± 7.5	12.03 ± 8.0
	2.33	0.50	100	2	1.02	120	480	360	1258.20	540	0.58 ± 3.7	5.84 ± 3.5
	2.33	0.50	100	4	1.02	120	420	300	1118.40	480	0.43 ± 3.5	4.36 ± 3.5
Cr(VI) ions (C_i)	2.33	0.50	100	1	1.02	180	900	720	2097.00	900	1.20 ± 7.5	12.03 ± 8.0
	2.33	0.50	100	1	2.60	120	600	480	1677.60	720	1.97 ± 6.4	19.77 ± 6.4
	2.33	0.50	100	1	5.05	90	540	450	1537.80	660	3.09 ± 21.5	30.93 ± 21.5

https://doi.org/10.1371/journal.pwat.0000528.t001

height, which dramatically reduced the contact between the PACW-active sites and chromium(VI) ion, resulting in lower column capacity. The reduction in such a column capacity could be mitigated by expanding the diameter of the column.

3.2.4. Effect of influent chromium(VI) concentration. Fig 8A depicts the influence of the chromium(VI) concentration on the biosorption capacity of PACW under constant pH, fluid flow rate, and height of the bed. The outcomes demonstrated that when the concentration of the influent ions was raised from 1.02 to 5.05 mg/L, the PACW bed saturated earlier, with the t_b dropping from 180 to 90 min (Table 1). Meanwhile, the column capacity increased from 12.03 ± 8.0 X 10^{-2} to 30.93 ± 21.5 X 10^{-2} mg/g. This was because the higher concentrations of chromium(VI) offered an enhanced driving force for biosorption due to the increase in concentration difference between the solution phase and the PACW interface, which increased the number of available chromium(VI) ions for the biosorption, thereby increasing the equilibrium column capacity [80–82]. This could also be explained based on an increased number of collisions between the PACW's reactive sites and the chromium(VI) ions, in addition to the higher mass transfer, which resulted in a greater proportion of biosorption [83]. Also, as the concentration of chromium(VI) ions was increased (5.05 mg/L), the percentage removal was 99.6 with the effluent chromium(VI) of 0.018 mg/L. This value is slightly greater than the tolerance limit suggested by the WHO. On the other hand, whenever the concentration was kept at a lower value (1.02 mg/L), the saturation was achieved more slowly, and the percentage removal was greater with the effluent chromium(VI) of 0.009 mg/L (S4 Data). This indicated that a lower influent chromium(VI) ion is more favorable for its effective removal from the aqueous phase in a column bed packed with the PACW.

3.3. Modeling the breakthrough profile

In the column investigations performed by the numerous researchers over the past decades, several expressions have been put forth for breakthrough curve analysis [84,85]. In this investigation, the Yoon-Nelson, the Adams-Bohart, the Bed Depth Service Time (BDST), as well as the Thomas models, were applied to examine the biosorbent-adsorbate interaction between the PACW and the chromium(VI) ions in the column bed [24]. The nonlinear forms of these models are generally employed to assess the closeness of observed values to the models; however, the correlation between the examined variables is complex, predicting the phenomena challenging. Conversely, in the linear representations of these models, the relationship between the examined variables can be readily illustrated by a simple linear equation, from which various column parameters are derived from the slope and intercept values [4]. Moreover, these models show how the chromium(VI) uptake performance of the biosorbent occurs over time by analyzing the experimentally recorded breakthrough curves, which are frequently utilized for the optimization of column parameters in continuous systems [65].

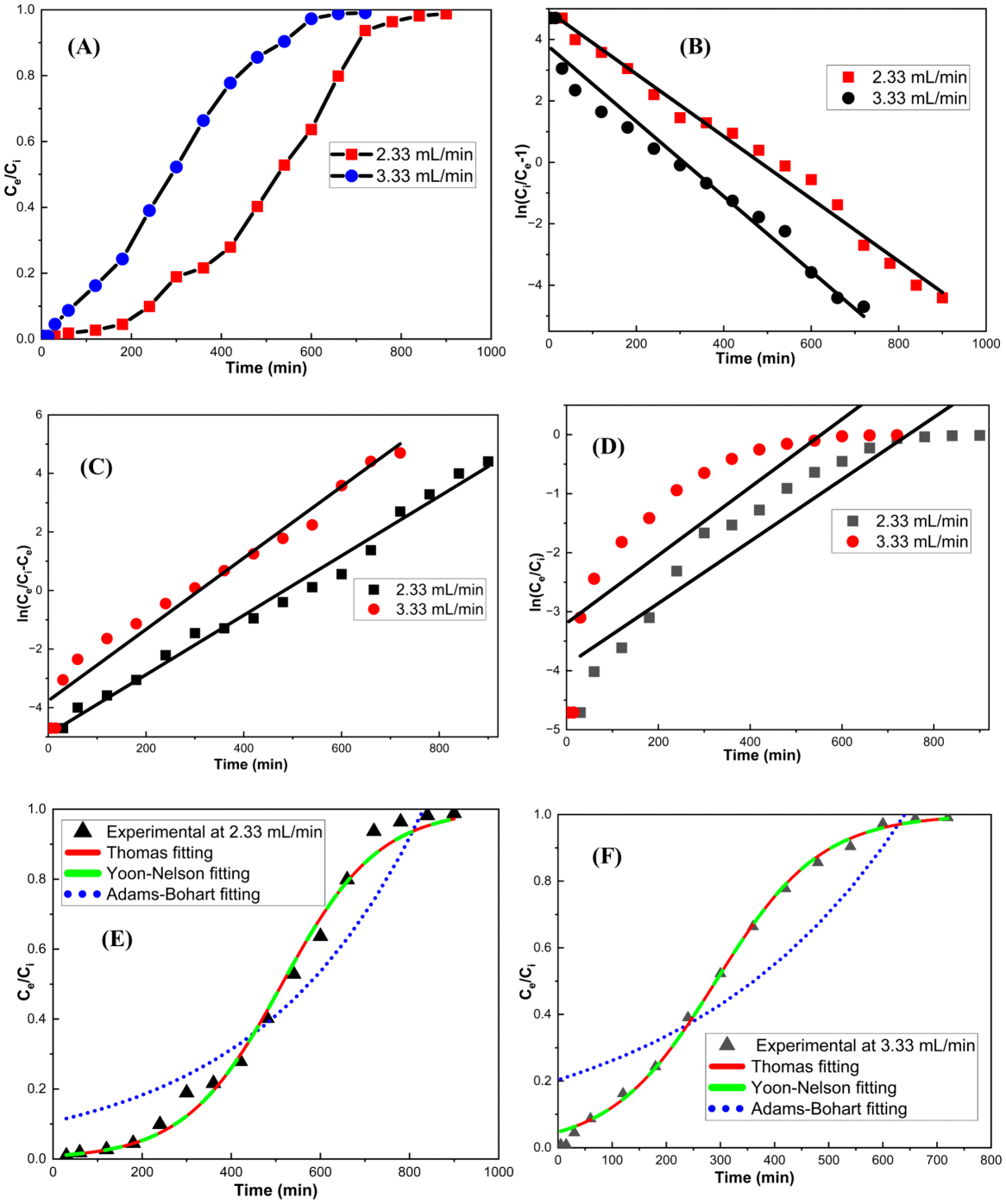


Fig 6. The breakthrough profiles of chromium(VI) ions at various fluid flow rates. (A) breakthrough plot of experimental data, (B) Thomas linear plot, (C) Yoon-Nelson linear plot, (D) Adams-Bohart linear plot and, (E & F) nonlinear plots of Thomas, Yoon-Nelson and Adams-Bohart expressions along with the experimental data (**condition**: pH = 1, influent concentration of chromium(VI) ions = 1.02 mg/L, fluid flow rates = 2.33-3.33 mL/min, and depth of the bed = 0.5 cm).

https://doi.org/10.1371/journal.pwat.0000528.g006

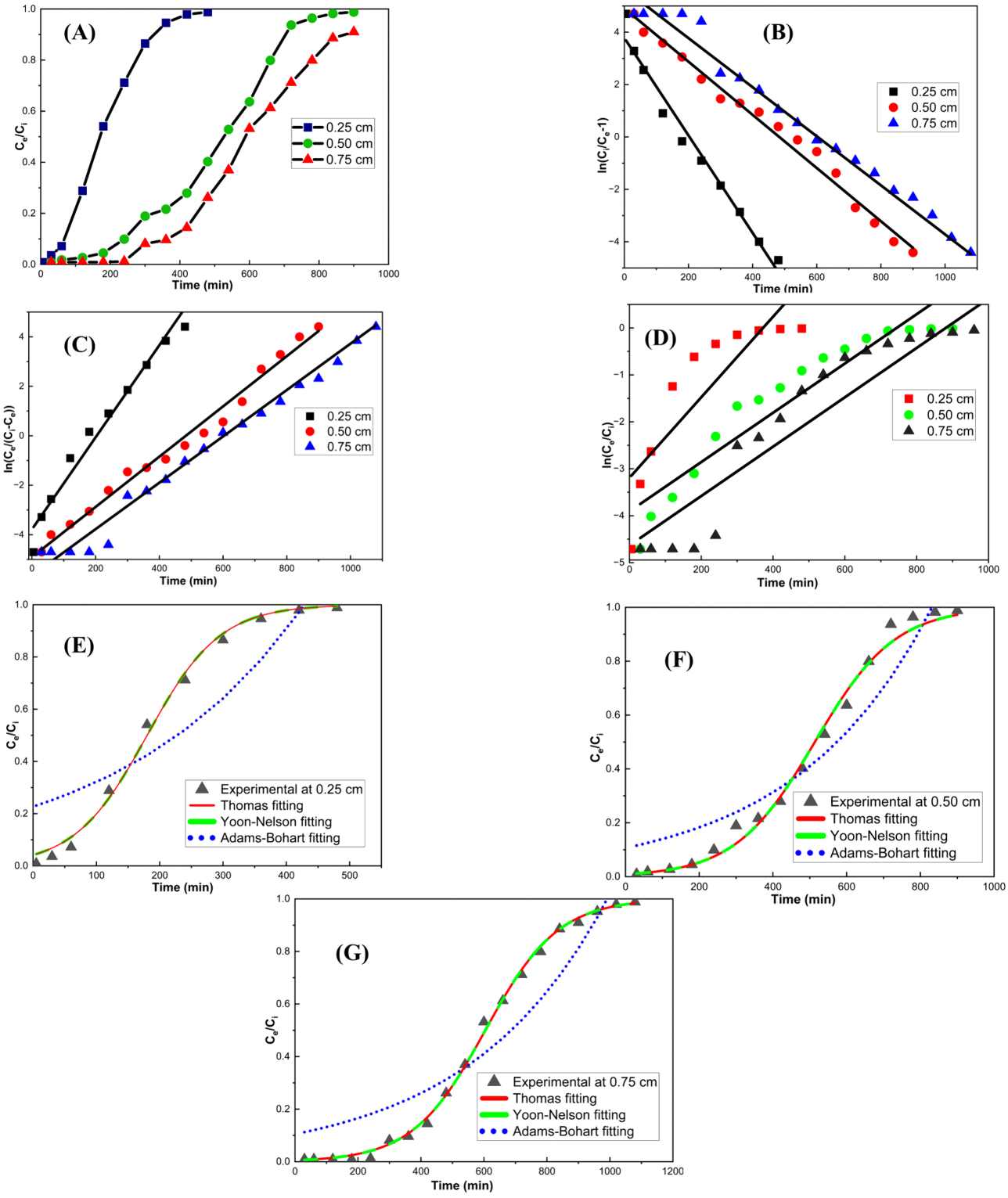


Fig 7. The breakthrough profiles of chromium(VI) ions at different depths of the bed. (A) breakthrough plot of experimental data, (B) Thomas linear plot, (C) Yoon-Nelson linear plot, (D) Adams-Bohart linear plot and, (E, F & G) nonlinear plots of Thomas, Yoon-Nelson and Adams-Bohart expressions along with the experimental data (**condition**: pH = 1, influent concentration of Cr(VI) ions = 1.02 mg/L, depth of the bed = 0.25-0.75 cm, and fluid flow rate = 2.33 mL/min).

https://doi.org/10.1371/journal.pwat.0000528.g007

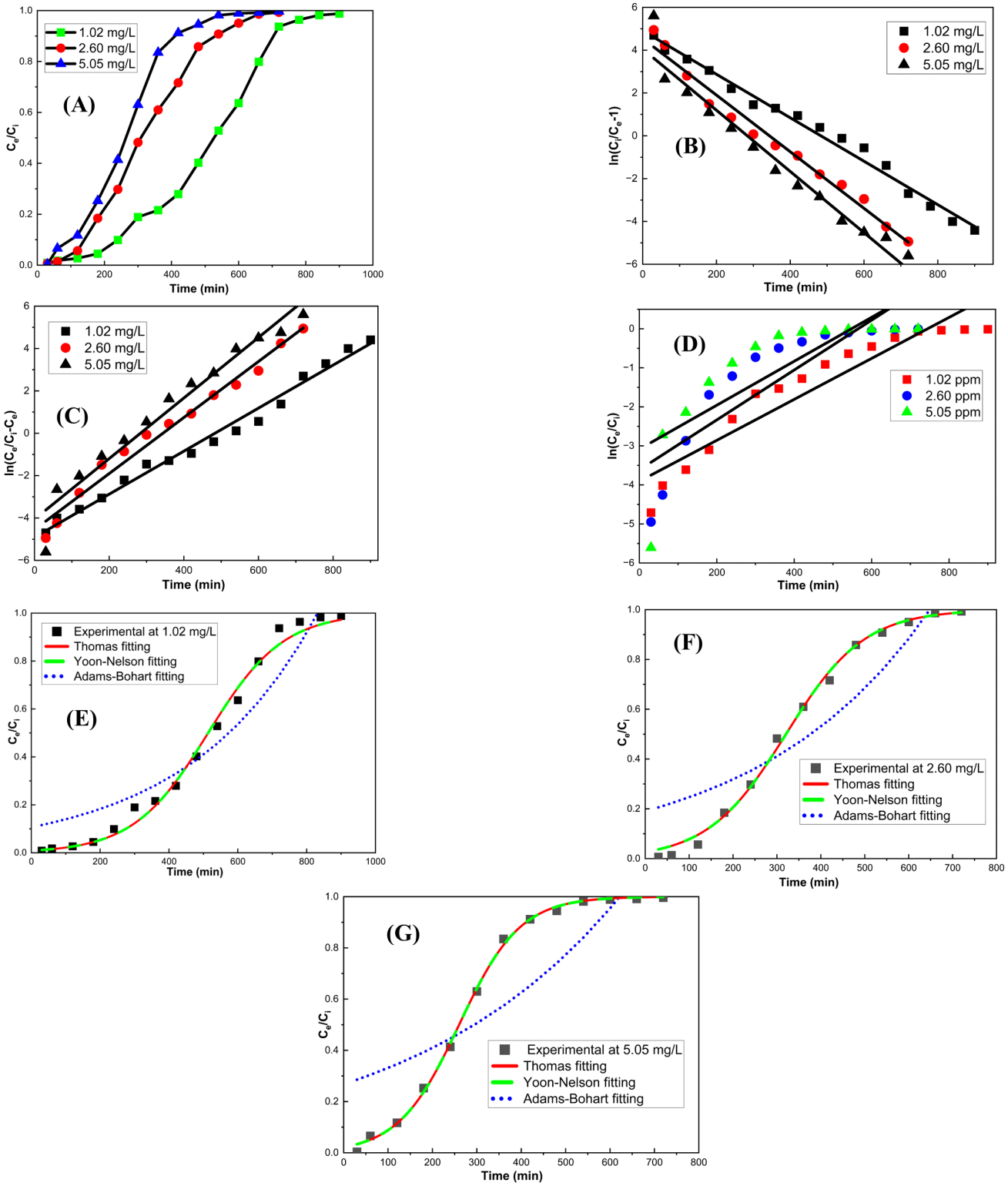


Fig 8. The breakthrough profiles of chromium(VI) ions at various concentrations. (A) a breakthrough plot of experimental data, (B) Thomas linear plot, (C) Yoon-Nelson linear plot, (D) Adams-Bohart linear plot and, (E, F & G) nonlinear plots of Thomas, Yoon-Nelson and Adams-Bohart expressions along with the experimental data (**condition**: pH = 1, influent concentration of Cr(VI) ions = 1.02 to 5.05 mg/L, fluid flow rate = 2.33 mL/min, and depth of the bed = 0.5 cm).

https://doi.org/10.1371/journal.pwat.0000528.g008

3.3.1. Thomas model. The model that describes the continuous biosorption performance in packed columns was first developed by Thomas in 1948 and has been extensively utilized to investigate the dynamics of adsorption in the column of a continuous system [86]. It has been commonly used to assess the adsorbent-adsorbate interaction, adsorption capacity, and rate constant, besides establishing other column parameters. Nonlinear as well as linear expressions of the Thomas model are expressed as follows [87,88]:

$$\frac{C_e}{C_i} = \frac{1}{1 + \exp\left(k_{Th}\frac{q_o M}{F} - k_{Th}C_i t\right)} \tag{11}$$

$$\ln\left(\frac{C_i}{C_e} - 1\right) = k_{Th}\frac{q_o M}{F} - k_{Th}C_i t \tag{12}$$

Here, M signifies the mass of the PACW in the column bed (g), C_i and C_e are incoming and outgoing concentrations of chromium(VI) ions in mg/L, k_{Th} signifies the Thomas rate constant in L/(mg min), and q_o signifies the optimum column capacity of the PACW bed for chromium(VI) ions in mg/g. Figures (5-8)B show the Thomas linear plots between ln[(C_i/C_e)-1] and t for different parameters using equation(12). Here, the plots yielded straight lines in each case with slopes of k_{Th} C_i and intercept values of $k_{Th}\frac{q_o M}{F}$, from which k_{Th} and q_o were computed. The values obtained are presented in Table 2.

The result from the linear modeling of the Thomas expression showed that while q_o reduced from 11.74 ± 0.16 to 10.76 ± 0.17 mg/g, k_{Th} increased from 9.7 X 10^{-3} ± 1.1 X 10^{-4} to 11.6 X 10^{-3} L/(min mg) with increasing the fluid flow rate from 2.33 to 3.33 mL/min. This is similar to the result obtained by Omitola et al [89]. The decrease in column capacity was due to the decrease in the contact time for the influent chromium(VI) ions [15]. Moreover, a rise in influent chromium(VI) ions from 1.02 to 5.05 mg/L resulted in an increase in q_o from 11.74 ± 0.16 to 33.61 ± 0.16 mg/g and a decrease in k_{Th} from 9.7 X 10^{-3} ± 1.1 X 10^{-4} to 2.8 X 10^{-3} ± 0.2 X 10^{-4} L/(min mg) [90]. This was because the increase in influent chromium(VI) concentration increased the concentration gradient among the chromium(VI) ions in the aqueous phase and the column, which ultimately created a driving force for the biosorption, thereby increasing the biosorption capacity [91]. Similar outcomes were recorded by Aksu and Gonen while utilizing the activated sludge for the biosorption of phenol [92]. Thus, it was concluded that a lower fluid flow rate, greater chromium(VI) concentration, moderate bed height (0.50 cm), and lower pH could probably increase the biosorption capacity in the column [40].

Table 2. Thomas parameters estimated from linear fitting in a column filled with PACW at different conditions (S5 Data).

Estimated column parameters		Thomas parameters			
		q_o (mg/g)	k_{Th} (L/mg min)	R^2	X2
Cr(VI) ion (C_i)	1.02	11.74 ± 0.16	9.7 X 10^{-3} ± 1.1 X 10^{-4}	0.98	0.11 ± 5.7 X 10^{-2}
	2.60	21.17 ± 0.23	5.0 X 10^{-3} ± 1.2 X 10^{-4}	0.98	0.20 ± 0.8 X 10^{-2}
	5.05	33.61 ± 0.16	2.8 X 10^{-3} ± 0.2 X 10^{-4}	0.95	0.54 ± 4.1 X 10^{-2}
Fluid flow rate (F)	2.33	11.74 ± 0.16	9.7 X 10^{-3} ± 1.1 X 10^{-4}	0.98	0.11 ± 5.7 X 10^{-2}
	3.33	10.76 ± 0.17	11.6 X 10^{-3}	0.96	0.32 ± 2.1 X 10^{-2}
Depth of bed (Z)	0.25	9.88 ± 0.16	17.6 X 10^{-3} ± 8.7 X 10^{-4}	0.97	0.29 ± 3.4 X 10^{-2}
	0.50	11.74 ± 0.16	9.7 X 10^{-3} ± 1.1 X 10^{-4}	0.98	0.11 ± 5.7 X 10^{-2}
	0.75	9.80 ± 0.09	8.8 X 10^{-3} ± 0.7 X 10^{-4}	0.98	0.15 ± 4.9 X 10^{-2}
pH of the solution	1	11.74 ± 0.16	9.7 X 10^{-3} ± 1.1 X 10^{-4}	0.98	0.11 ± 5.7 X 10^{-2}
	2	5.94 ± 0.26	16.0 X 10^{-3} ± 7.9 X 10^{-4}	0.98	0.14 ± 1.6 X 10^{-2}
	4	4.27 ± 0.16	16.5 X 10^{-3} ± 3.2 X 10^{-4}	0.97	0.18 ± 12.6 X 10^{-2}

https://doi.org/10.1371/journal.pwat.0000528.t002

Furthermore, from the analysis of the table, it was discovered that the biosorption capacities estimated from the linear forms of the Thomas model were closer to the values determined experimentally in each of the cases, where the coefficients of determination (R^2) were always greater than 0.95, with significantly lower values of X2 in all the cases.

Figures 5, 7 & 8(E, F & G) and Figs 6(E & F) (red line) demonstrate the nonlinear fitting of experimental values for the variation of several parameters in a fixed bed during the chromium(VI) removal process. The outcomes of the nonlinear fitting data are shown in supplementary table 2 (S2 Table), which also shows an analogous trend to that in the case of linear modeling. Here, the biosorption capacities are similar to the experimental values with the $R^2 > 0.97$ and $\chi 2$ values minimum [48] for all the conditions. This demonstrated that the Thomas model could precisely describe the chemical interaction within the column bed filled with the PACW in a continuous system. This finally concluded that the diffusion of chromium(VI) was not primarily happening during the chromium(VI) biosorption in the packed column bed [3,80,92,93].

3.3.2. The Yoon-Nelson modeling. Yoon and Nelson developed a fundamental equation [94] for the description of breakthrough data obtained from the biosorption of gases on activated carbon. It is a semi-empirical model, which helps to minimize the errors of the Thomas model. According to this model, a detailed comprehension of the physicochemical characteristics of materials is deemed unnecessary; and is based on the theory that each adsorbate molecule's rate of decrease in adsorption potential is correlated with both the "probability of adsorption and the probability of breakthrough on the adsorbent". Generally, this model helps to estimate the column parameters, such as 50% saturation time and the rate of biosorption. Linear (equation(13)) and nonlinear (equation(14)) forms of this model can be expressed as follows:

$$\ln\left(\frac{C_e}{C_i - C_e}\right) = k_{YN}t - k_{YN}\tau \tag{13}$$

$$\frac{C_e}{C_i} = \frac{1}{1 + \exp\left(k_{YN}\tau - k_{YN}t\right)} \tag{14}$$

Here, t represents the processing time (min), τ represents the time needed for 50% saturation (min), whereas k_{YN} denotes the Yoon-Nelson rate constant in min^{-1}. Figures (5-8)C depict the Yoon-Nelson linear plots of $\ln\left(\frac{C_e}{C_i - C_e}\right)$ *versus* t for various pHs, fluid flow rates, biosorbent doses, and initial chromium(VI) concentrations. In the present investigation, equation(13) always gave straight lines, where the k_{YN} and the τ, for all the plots, were estimated from the slope and the intercept, respectively. The calculated values are listed in Table 3.

It was evidenced from the table that, whenever the PACW amount was raised from 50 mg to 150 mg, the τ increased proportionally from 3.43 ± 0.06 to 10.25 ± 0.11 hours, accompanied by a reduction in the k_{YN} values from 18.1 ± 0.87 to 9.1 ± 0.10 min^{-1}. It was also revealed that, when the influent concentration of chromium(VI) was dropped from 5.05 to 1.02 mg/L, the K_{YN} decreased from 14.2 ± 0.17 to 10.1 ± 0.24 min^{-1}; however, the τ value increased from 4.74 ± 0.03 to 8.06 ± 0.15 hours. This suggested that the increase in PACW amount and decline in the influent chromium(VI) concentration leads to the biosorption of chromium(VI) with the prolonged saturation time and lower k_{YN} values [95]. An analogous trend was noticed whenever the fluid flow rate was decreased from 3.33 to 2.33 mL/min. This pointed out that there was a mass transfer inside the column, which was due to the dispersion during the biosorption process at the lower effluent concentration, higher biosorbent amount, and a lower fluid flow rate.

Moreover, while analyzing the experimental data by utilizing this model, it was noticed that the values of R^2 were at least 0.95 if all the data were considered.

Also, in the nonlinear fitting of this model [green dashed line in the Figs 5, 7 & 8(E, F & G) and the Figs 6(E & F)], the data obtained from the model closely fitted with the breakthrough curve of the experimental data with $R^2 > 0.97$ for all the process variables that were evaluated (S3 Table). This indicated that the linear as well as nonlinear forms of this model

Table 3. Yoon-Nelson parameters estimated from linear fitting in a column filled with PACW at different conditions (S6 Data).

Estimated column parameters		Yoon-Nelson parameters			
		X (hour)	k_{YN}/min	R^2	X2
Cr(VI) ion (C_i)	1.02	8.06 ± 0.15	10.1 ± 0.24	0.98	0.11 ± 5.8 X 10^{-2}
	2.60	5.73 ± 0.08	13.2 ± 0.36	0.98	0.20 ± 0.8 X 10^{-2}
	5.05	4.74 ± 0.03	14.2 ± 0.17	0.95	0.54 ± 4.1 X 10^{-2}
Fluid flow rate (F)	2.33	8.06 ± 0.15	10.1 ± 0.24	0.98	0.11 ± 5.8 X 10^{-2}
	3.33	5.21 ± 0.07	12.0 ± 0.05	0.96	0.32 ± 2.1 X 10^{-2}
Depth of bed (Z)	0.25	3.43 ± 0.06	18.1 ± 0.87	0.97	0.29 ± 3.4 X 10^{-2}
	0.50	8.06 ± 0.15	10.1 ± 0.24	0.98	0.11 ± 5.8 X 10^{-2}
	0.75	10.25 ± 0.11	9.1 ± 0.10	0.98	0.15 ± 4.9 X 10^{-2}
pH of the solution	1	8.06 ± 0.15	10.1 ± 0.24	0.98	0.11 ± 5.8 X 10^{-2}
	2	4.12 ± 0.13	16.5 ± 0.70	0.98	0.14 ± 1.7 X 10^{-2}
	4	2.95 ± 0.09	17.1 ± 0.30	0.97	0.18 ± 12.7 X 10^{-2}

https://doi.org/10.1371/journal.pwat.0000528.t003

were capable of describing the chromium(VI) removal process in the column bed adequately [96]. Thus, it was concluded that the model was able to describe the rate of biosorption accurately.

3.3.3. Adams-Bohart model. Adams–Bohart equation is a mathematical expression which postulates that biosorption is a slow process and is regulated by external mass transfer [97]. This model is extensively applied to estimate N_o, the saturated biosorption ability, as well as k_{AB}, the mass transfer rate constant [80]. Also, the model is typically applied to examine the initial part of a breakthrough curve where $C_e/C_i < 0.5$ [40,98,99]. The following expressions are employed to represent the linear as well as nonlinear equations of this model [97]:

$$\ln\left(\frac{C_e}{C_i}\right) = k_{AB}C_i t - k_{AB}N_o\frac{Z}{U_o} \tag{15}$$

$$\frac{C_e}{C_i} = \frac{1}{\exp\left(\frac{k_{AB}N_oZ}{U_o} - k_{AB}C_i t\right)} \tag{16}$$

Here, N_o signifies the saturated biosorption capacity in mg/L, Z represents the height of the bed in cm, K_{AB} signifies the mass transfer coefficient (L/(mg min)), C_i and C_e represent the influent and the concentration of chromium(VI) (mg/L) at time t (min), respectively, and U_o is the fluid flow rate or linear velocity in cm/min.

Figures (5-8)D display breakthrough curves fitting with the linear version of the Adams-Bohart expression, and the calculated data of the variables designed by the model are presented in Table 4.

When all the experimental data were plotted against the linear form of the Adams-Bohart model, it showed a minimum value of coefficient of determination ($R^2 = 0.62$, Fig 8D) at the influent concentration of 5.05 mg/L, whereas it exhibited a maximum value of coefficient of determination ($R^2 = 0.89$) at the influent concentration of 1.02 mg/L. This suggested that the model could not be considered suitable for the present condition and thus could be employed only at the earliest stages of the experiment [15]. Also, as seen in the table, k_{AB} increased from 5.1 X 10^{-3} ± 1.1 X 10^{-4} to 5.6 X 10^{-3} ± 1.1 X 10^{-4} L/(min mg) with a rise in fluid flow rate from 2.33 to 3.33 mL/min, and reduced from 8.3 X 10^{-3} ± 5.2 X 10^{-4} to 5.1 X 10^{-3} ± 0.6 X 10^{-4} L/(min mg) and from 5.1 X 10^{-3} ± 1.1 X 10^{-4} to 1.1 X 10^{-3} ± 0.1 X 10^{-4} L/(min mg) with the rise in depth from 0.25 to 0.75 cm and influent concentration from 1.02 to 5.05 mg/L, respectively. This outcome is analogous to the results obtained by Aksu and Gonen [92], signaling that the chromium(VI) biosorption was guided by external mass transfer [100,101].

Table 4. Adams-Bohart parameters estimated from linear fitting in a column filled with PACW at different conditions (S7 Data).

Estimated column parameters		Adams-Bohart parameters			
		N_o (mg/L)	k_{AB} (L/mg min)	R^2	X2
Cr(VI) ion (C_i)	1.02	7081.81 ± 14.9	5.1 X 10^{-3} ± 1.1 X 10^{-4}	0.89	0.26 ± 1.5 X 10^{-2}
	2.60	13651.88 ± 15.0	2.4 X 10^{-3} ± 0.1 X 10^{-4}	0.76	0.75 ± 0.8 X 10^{-2}
	5.05	25618.77 ± 15.5	1.1 X 10^{-3} ± 0.1 X 10^{-4}	0.62	1.10 ± 1.0 X 10^{-2}
Fluid flow rate (F)	2.33	7081.81 ± 14.9	5.1 X 10^{-3} ± 1.1 X 10^{-4}	0.89	0.26 ± 1.5 X 10^{-2}
	3.33	7556.94 ± 21.8	5.6 X 10^{-3} ± 1.1 X 10^{-4}	0.74	0.75 ± 1.3 X 10^{-2}
Depth of bed (Z)	0.25	7086.00 ± 41.2	8.3 X 10^{-3} ± 5.2 X 10^{-4}	0.74	0.80 ± 31.2 X 10^{-2}
	0.50	7081.81 ± 14.9	5.1 X 10^{-3} ± 1.1 X 10^{-4}	0.89	0.26 ± 1.5 X 10^{-2}
	0.75	5595.40 ± 17.4	5.1 X 10^{-3} ± 0.6 X 10^{-4}	0.87	0.48 ± 3.4 X 10^{-2}
pH of the solution	1	7081.81 ± 14.2	5.1 X 10^{-3} ± 1.1 X 10^{-4}	0.89	0.26 ± 1.5 X 10^{-2}
	2	4068.89 ± 21.4	7.7 X 10^{-3} ± 2.1 X 10^{-4}	0.81	0.55 ± 3.5 X 10^{-2}
	4	3669.70 ± 6.8	5.6 X 10^{-3} ± 2.2 X 10^{-4}	0.82	0.21 ± 2.1 X 10^{-2}

https://doi.org/10.1371/journal.pwat.0000528.t004

Besides, when the experimental values were plotted with the nonlinear equation of the Adams-Bohart expression (S4 Table), as shown by the dotted blue line in the Figures 5, 7 & 8(E, F & G) and 6(E & F), the plots were extremely far from the fitting with the observed data. This suggested that the Adams-Bohart model was inadequate to deduce the correlation between the biosorbent and the chromium(VI) ions accurately [42].

3.3.4. BDST model. It is a mathematical expression where the kinetic parameters in a fixed bed are determined from the graphical plot of the bed depth (Z) as a function of breakthrough service time (t_B). This mathematical expression has been utilized frequently for the initial part of the breakthrough plots as well as to estimate the design parameters for the biosorption column. The relationship expressed in equation(17) has been used to represent the BDST model [102,103].

$$t_B = \frac{N_o}{C_i U_o} Z - \frac{1}{k_{BDST} C_i} \ln\left(\frac{C_i}{C_B} - 1\right) \tag{17}$$

Here, the variables C_i and C_B denote the incoming and outgoing concentrations of chromium(VI) ions in the column (mg/L), respectively, N_o stands for the biosorption potential or saturation capacity (mg/L), Z (cm) indicates the height of the bed, whereas U_o indicates the linear velocity (cm/min) within the fixed bed, and k_{BDST} is the rate constant in L/(mg min). In this study, a straight line plot was obtained when the experimental values of t_B and the Z were plotted (Fig 9).

From the analysis, the k_{BDST} for bed heights of 0.25, 0.50, and 0.75 cm were evaluated to be 0.124, 0.149, and 0.196 L/(mg min), respectively, whereas the value of the biosorption potential of chromium(VI) was calculated to be 1711.80 mg/L with the coefficient of determination (R^2) higher than 0.96 (S8 Data). These findings confirmed that the BDST model appropriately represented the investigated biosorption system; thus, the model could be applied and considered to be reliable in designing the column parameters, such as the depth of the bed, breakthrough time, volumetric flow rate, and initial concentration [104].

3.4. Mechanism of biosorption

From the new peak evidenced at 1654.92 cm^{-1} corresponding to the C = O stretching vibration on the FTIR spectroscope, it was proved that there was a new functional group created due to the ring opening reaction that took place during the acid treatment of ACW. Also, at the pH around 1, there were maximal $HCrO_4^-$ ions present in the aqueous solution [75] due to which, there was a strong interaction between the $HCrO_4^-$ anions and the PACW surface, which caused the biosorption of these ions onto the PACW surface through a complexation reaction (S1 Scheme, step 3). Moreover, the data of EDX

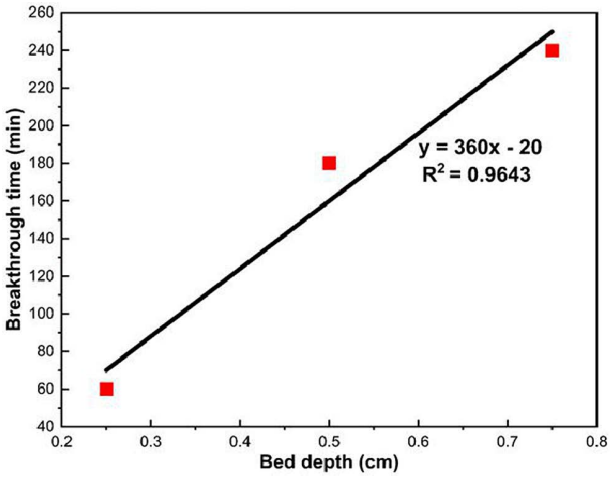


Fig 9. BDST plot illustrating the correlation between the depth of the bed and breakthrough service time.

https://doi.org/10.1371/journal.pwat.0000528.g009

analysis (Fig 3B) showed a peak at the binding energy of approximately 5.40 keV corresponding to the elemental chromium, which demonstrated that the chromium(VI) was successfully biosorbed onto the PACW.

In the isotherm plot of the BET analysis (S1A Fig), it was discovered that at the lower pressure (0.0068-0.0585 Pa), the biosorption of N_2 gas on the surface of PACW was faster due to the easily available surface, which led to a monolayer surface coverage attaining a faster equilibrium. Furthermore, the good fit of the Thomas model concluded that the phenomenon was not diffusion controlled, whereas the better fitting of the Yoon-Nelson model established that the biosorbent-adsorbate contact was primarily a mass transfer process among the adsorbate ions in the aqueous phase and the biosorbent.

3.5. Application of a packed column of PACW for the treatment of industrial effluent

A water sample was brought with permission from the Everest dyeing industry, a local carpet factory in Jorpati, Kathmandu, Nepal, to evaluate the true efficacy of the PACW to effectively treat the water containing chromium(VI). Various types of woolen threads are dyed in this factory, which are used to create varieties of carpets in Nepal. First, as mentioned here, the physicochemical properties of the water sample were calculated. [Chloride = 90.94 mg/L, ammonia = 5 mg/L, sulphate = 30.16 mg/L, calcium = 480.40 mg/L, magnesium = 80.40 mg/L, bicarbonate = 280 mg/L, turbidity = 60.33 NTU, conductivity = 270 μS/cm, total hardness = 1560 mg/L, and chromium(VI) = 49.98 mg/L]. To make the study comparable with the findings from the earlier study on the simulated water, the water was diluted to make 2.30 mg/L of chromium(VI) while keeping the pH at 1. The procedure was then repeated as stated in **section 2.4**, and Fig 10 displays the breakthrough profile. It can be seen in the figure that by using merely 100 mg, the PACW can effectively reduce the chromium(VI) from 2.30 mg/L to 0.10 mg/L, which is the WHO requirement for effluent water. The maximum loading capacity (q_{equ}) here is 12.00 mg/g, which is somewhat less than that of the simulated water ($q_{equ} = 19.77 \pm 6.4 \text{ X } 10^{-2}$ mg/g) at an influent concentration of 2.60 mg/L under identical conditions. One possible explanation for the lower q_{equ} value may be the interferences brought on by the different ions present in the industrial effluent. This concluded that the PACW could effectively biosorb and remove traces of chromium(VI) ions from industrially contaminated water, thereby upholding the water safety standard as recommended by the WHO.

3.6. Possibility of regeneration and recycling

It was observed in the batch experiment that over 93% of the biosorbed chromium(VI) was desorbed successfully by a 2 M NaOH solution, as shown in supplementary figure 3 (S3 Fig) [62]. Therefore, it is reasonable to think that the column

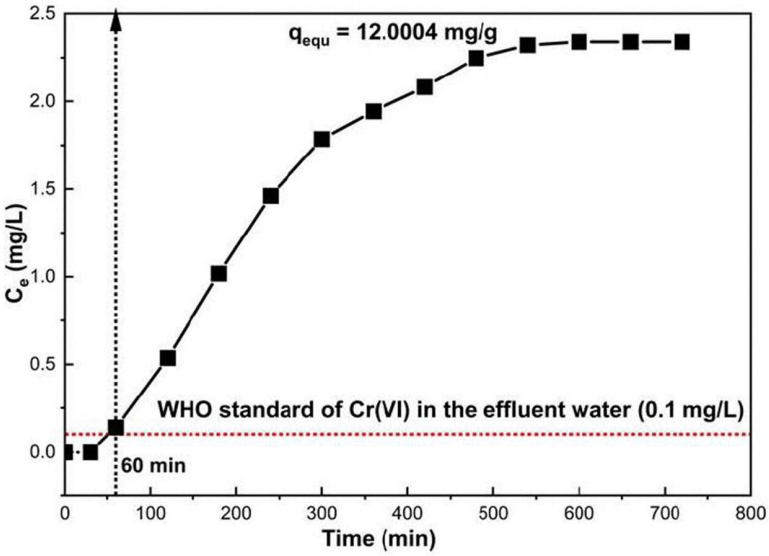


Fig 10. Breakthrough diagram of industrial water. Condition: influent concentration of chromium(VI) or Cr(VI) = 2.30 mg/L, fluid flow rate = 2.33 mL/min, bed height = 0.50 cm, and pH = 1.

https://doi.org/10.1371/journal.pwat.0000528.g010

bed can be washed with a diluted NaOH solution to regenerate the spent biosorbent once the column experiment is completed. The chromium(VI) can be recovered from the filtrate; however, the washed biosorbent can be reutilized after reconditioning for the next round of column test by passing fresh chromium(VI) ions into the column.

3.7. Comparative analysis using alternative biosorbents

Table 5 demonstrates the comparison of chromium(VI) biosorption capacities of variously reported biosorbents in a column packed with the fixed bed with that of PACW, which was examined in this work.

In the table, it is evident that the chromium(VI) uptake capacity of the column is affected by the nature of the material used, pH, fluid flow rate, depth of the column, and the initial concentration of the chromium(VI) ions. Also, it can be noticed that the chromium(VI) uptake in the column is good at lower pH values. Moreover, it can be seen that the chromium(VI) uptake capacity of PACW with 1.02 mg/L of influent chromium(VI) ions is far greater than the activated charcoal [53], rice husk [41], earth material [44], natural mineral [45], *Swietenia mahagoni* [51], Zeolite NaX [52] and *Psidium guajava* leaves [105] at the bed height of just 0.5 cm. Also, PACW shows greater biosorption capacity than the titanium oxide nanoparticle [42] and the lime rock [44] with merely an influent concentration of 2.60 mg/L. Moreover, PACW surpasses the biosorption capacity of the waste acorn of *Quercus ithanburensis,* which is just 30.23 mg/g at 100 mg/L of influent concentration and 10 cm of bed depth [39]. From this analysis, it was concluded that PACW had a great potential for reducing lower values of chromium(VI) concentrations in contaminated water sources and, hence, could be considered a promising material to remove chromium(VI) ions from a continuous system.

3.8. Economic feasibility and scaling of biosorbent column

It was observed that PACW could effectively perform in a small scale continuous column operation when utilized in a modeled solution. For bed heights of 0.25 cm, 0.50 cm, and 0.75 cm, a total of 8, 15, and 18 hours, respectively, were adequate if a fluid flow rate of 140 mL/h (3.36 L/day) was maintained. Therefore, PACW with a medium-sized pilot scale column (100 L capacity) and its treatment with real contaminated water could constitute the next-phase research. Once

Table 5. A comparative study of equilibrium column capacity for chromium(VI) evaluated for different biosorbents, with PACW.

S.N.	Adsorbent	pH	F (mL/min)	Z (cm)	C_i (mg/L)	q_{equ} (mg/g)	References
1	Activated charcoal (*Sapindus trifoliate L.)*	7.2	0.5	15	10	1.71	[53]
2	Hydrotalcite derived adsorbent	6	1	–	50	36.4	[38]
3	Waste acorn of *Quercus ithanburensis*	2	5	10	100	30.23	[39]
4	Modified corn stalk	4.9	15	1.4	200	67.45	[40]
5	Rice husk	2	30	10	20	11.04	[41]
6	Titanium(IV) oxide nanoparticle	2	1	4	32	12.94	[42]
7	Tea factory waste	2	10	10	50	27.67	[43]
8	Herbal waste based biochar (BC)	2	3	2	20	20.00	[3]
9	Lime rock for tannery wastewater	2	2.5	5	150	12.70	[44]
10	Earth material (gravel particle)	4	2.5	5	150	2.30	[44]
11	Mexicalcite (natural mineral)	7	2	4	75	4.96	[45]
12	Rice bran	2	20	15	30	19.81	[46]
13	Sago bark	3	4	6	1000	35.82	[47]
14	Almond shell	3.7	3	7	67.5	21.92	[48]
15	Activated neem bark	2	10	--	100	35.08	[49]
16	Rice husk ash	2.5	5	2.5	150	73.30	[50]
17	H_3PO_4 modified *Swietenia mahagoni*	2	5	9	50	10.82	[51]
18	H_2SO_4 modified *Swietenia mahagoni*	2	5	9	50	9.08	[51]
19	Zeolite NaX	4	13.75	15.24	10	5.66	[52]
20	*Psidium guajava* leaves	–	40	10	20	8.72	[105]
21	PACW at pH 1	1	2.33	0.50	1.02	12.03	**This study**
22	PACW at pH 2	2	2.33	0.50	1.02	5.84	**This study**
23	PACW at pH 4	4	2.33	0.50	1.02	4.36	**This study**
24	PACW at F = 3.33 mL/min	1	3.33	0.50	1.02	10.13	**This study**
25	PACW at Z = 0.25 cm	1	2.33	0.25	1.02	8.90	**This study**
26	PACW at Z = 0.75 cm	1	2.33	0.75	1.02	9.69	**This study**
27	PACW at Cr(VI) = 2.6 mg/L	1	2.33	0.50	2.60	19.77	**This study**
28	PACW at Cr(VI) = 5.05 mg/L	1	2.33	0.50	5.05	30.93	**This study**

https://doi.org/10.1371/journal.pwat.0000528.t005

the chromium(VI) biosorption system is successfully scaled up in a pilot plant, it could be implemented in a large industrial scale PACW column to remove chromium(VI) ions from contaminated water. To evaluate the practical viability of the investigated system, an economic assessment was necessary. In the present work, the authors utilized the waste biomass of *A. catechu* as a feed material, which required minimal chemical input. From the process, it was found that NRs. 300 were sufficient to synthesize 1 kilogram of biosorbent from the ACW. This included all the major expenses such as raw ACW (5 NRs/kg), orthophosphoric acid (NRs. 500/L), and electricity (NRs. 12/kWh). Also, it was observed that the operational costs and usage of other chemicals, such as HCl and NaOH solutions, were very low, due to which, cost evaluation was not essential. Hence, it was concluded that the overall treatment cost for chromium(VI) contaminated water could be reduced by employing PACW as a packing material in a column of a fixed bed setting.

4. Conclusion

This work developed a novel biosorbent from *A. catechu* waste by H_3PO_4 activation, followed by carbonization to get PACW for chromium(VI) treatment from an aqueous solution. The records of the FTIR spectroscope supported the ring

opening reaction of the ACW and shift of wavenumber in the FTIR spectroscope after the treatment with the chromium(VI) supported the binding of chromium(VI) onto the PACW. Also, a new peak due to chromium(VI) discovered in the EDX analysis revealed that it was efficiently biosorbed onto the PACW through a complexation reaction. During the test, different column parameters were examined, from which it was found that the biosorption performance was maximum at pH 1. At the influent concentration of 1.02 mg/L and a column depth of 0.50 cm, the chromium(VI) removal efficacy was maximum and determined to be 12.03 ± 8.0 X 10^{-2} mg/g, consequently fulfilling the WHO's standard of upper limit (0.05 mg/L) for the drinkable water. With raising the fluid flow rate from 2.33 to 3.33 mL/min, the column capacity decreased from 12.03 ± 8.0 X 10^{-2} to 10.13 ± 9.5 X 10^{-2} mg/g from the water, and the equilibrium reached faster. Contrarily, by elevating the influent concentration from 1.02 to 5.05 mg/L, the equilibrium column capacity increased from 12.03 ± 8.0 X 10^{-2} to 30.93 ± 21.5 X 10^{-2} mg/g, but the removal efficiency was less, and the water quality standard could not meet the level as recommended by the WHO. Hence, the low concentration of influent chromium(VI), the moderate depth of the column, and the lower pH and fluid flow rate offered better results in the packed column bed.

Four mathematical expressions were utilized to explain the experimental breakthrough curves, where the experimental data were better explained by the Thomas, the Yoon-Nelson, and the BDST models, with R^2 values more than 0.95 in each condition. The highest biosorption capacity derived from the Thomas linear model was 33.61 ± 0.16 mg/g, which was closer to the experimental result. Additionally, through the use of 100 mg of PACW, it was able to successfully biosorb 12.00 mg/g of chromium(VI) from the effluent and was able to reduce its amount to 0.10 mg/L, satisfying the WHO's requirement for industrial runoffs. Therefore, PACW could be regarded as an appropriate biosorbing material to remove chromium(VI) from columns packed in a fixed bed due to its moderate biosorption ability, as compared to the majority of biosorbents considered in this paper.

Supporting information

S1 File. Graphical Abstract.
(TIF)

S1 Fig. Results obtained from the BET analysis (A) biosorption-desorption isotherm of N_2 at 77.35 K, (B) surface area, (C) volume occupied by pores ranging from 0 to 50 nm, (D) pore volume distribution & (E) pore surface area distribution curves.
(TIF)

S1 Scheme. Synthetic route of PACW from ACW. Step 1: synthesis of PACW; step 2: protonation of PACW at low pH; step 3: complexation of chromium(VI) ion, and desorption of chromium(VI) to regenerate the PACW
(TIF)

S2 Fig. Zeta potential *versus* pH plot to determine the pH_{PZC} of PACW.
(TIF)

S3 Fig. % Desorption of chromium(VI) from chromium(VI) loaded PACW with various concentrations of NaOH solution.
(TIF)

S1 Table. Surface properties of PACW obtained from BET analysis. Here, S_{BET} (m^2/g) represents a total surface area from the BET equation, S_{micro} (m^2/g) denotes the surface area of the micropores, S_{meso} (m^2/g) represents the surface area of the mesopores calculated by subtracting the S_{micro} from the $S_{BET,}$ S_{ext} (m^2/g) is the external surface area, V_{total} (cm^3/g) is the total volume occupied by the micro and mesopores, V_{micro} (cm^3/g) is the volume occupied by the micropores, V_{meso} (cm^3/g) represents the mesopore volume and, APD (nm) is the average diameter of the pores.
(XLSX)

S2 Table. Thomas nonlinear fitting. Here, Z denotes the height of the bed (cm), F represents the fluid speed (mL/min), C_i signifies the initial chromium(VI) concentration (mg/L), q_o denotes the Thomas adsorption capacity mg/g), k_{Th} represents the Thomas constant (L/mg min), X2 denotes the reduced chi-square, and R^2 is the coefficient of determination.
(XLSX)

S3 Table. Yoon-Nelson nonlinear fitting. Here, k_{YN} represents the Yoon-Nelson constant (min^{-1}), and X denotes the time (min) required to breakthrough 50% of the material (PACW).
(XLSX)

S4 Table. Adams-Bohart nonlinear fitting. Here, k_{AB} denotes the Adams-Bohart constant (mL/(min mg)), and N_o represents the saturated adsorption capacity (mg/L) derived from the Adams-Bohart model.
(XLSX)

S1 Data. BET analysis of column investigation using PACW.
(XLSX)

S2 Data. FTIR and XRD values of ACW, PACW and Cr(VI)-PACW.
(XLSX)

S3 Data. Triplicate data and the evaluation of q_{total} and q_{equ} in the fixed bed of PACW at the continuous fluid flow of Cr(VI) solution.
(XLSX)

S4 Data. Triplicate data of various column parameters in a fixed bed PACW at the continuous fluid flow of Cr(VI) solution.
(XLSX)

S5 Data. Triplicate data and the statistical analysis to evaluate the Thomas parameters of Cr(VI)-PACW bed.
(XLSX)

S6 Data. Triplicate data and the statistical analysis to evaluate the Yoon-Nelson parameters of Cr(VI)-PACW bed.
(XLSX)

S7 Data. Triplicate data and the statistical analysis to evaluate the Adams-Bohart parameters of Cr(VI)-PACW bed.
(XLSX)

S8 Data. Statistical analysis on the BDST model for the Cr(VI)-PACW bed at three sets of column heights.
(XLSX)

Acknowledgments

The authors express their gratitude to Debendra Acharya, a doctoral researcher, and Dr. Kishan Chhetri, Jeonbuk National University (South Korea), for EDX & SEM analyses. The authors also express their indebtedness to Dr. Sabita Shrestha, Central Department of Chemistry, Tribhuvan University, Kirtipur, Kathmandu, Nepal, for the digital measurement of FTIR. The authors are also grateful to Dr. Swagat Shrestha, Amrit Science Campus, Thamel, Kathmandu, Nepal, for providing a lab facility for carbonization.

Author contributions

Conceptualization: Prabin Basnet, Kedar Nath Ghimire.

Data curation: Prabin Basnet.

Formal analysis: Prabin Basnet.

Investigation: Prabin Basnet.

Project administration: Hari Paudyal.

Supervision: Hari Paudyal.

Validation: Kedar Nath Ghimire, Hari Paudyal.

Writing – original draft: Prabin Basnet.

Writing – review & editing: Prabin Basnet, Hari Paudyal.

References

1. Basnet P, Gyawali D, Nath Ghimire K, Paudyal H. An assessment of the lignocellulose-based biosorbents in removing Cr(VI) from contaminated water: A critical review. Results Chem. 2022;4:100406.
2. Rim I, Hezil N, Fellah M, Saoudi A, Aleksei O, El-Hiti GA. Enhancing kaolin performance through organic molecule modification and assessing its efficiency for lead and copper adsorption. Environmental Technology & Innovation. 2024;36:103904.
3. Pawar S, Uma K, Theodore T. Development of biochar using herbal industry waste for removal of hexavalent chromium from aqueous solution: Column study. Results in Chemistry. 2024;10:101713. https://doi.org/10.1016/j.rechem.2024.101713
4. Hezil N, Fellah M, Montagne A, Iost A, Obrosov A, Weiss S. Removal of Chromium (VI) from Water onto Activated Carbon by Adsorption in Dynamic Mode. The Minerals, Metals & Materials Series. Springer International Publishing. 2020. 855–63. https://doi.org/10.1007/978-3-030-36296-6_80
5. Abebe A. Impacts of chromium from tannery effluent and evaluation of alternative treatment options. 2010. https://repository.ju.edu.et//handle/123456789/3275
6. Cieślak-Golonka M. Toxic and Mutagenic Effects of Chromium (VI). A Review. Polyhedron. 1996;15(21):3667–89. https://www.sciencedirect.com/science/article/pii/0277538796001416
7. World Health Organization. Guidelines for Drinking-Water Quality: Fourth Edition Incorporating the First and Second Addenda. 2024.
8. Kang S-Y, Lee J-U, Moon S-H, Kim K-W. Competitive adsorption characteristics of Co2+, Ni2+, and Cr3+ by IRN-77 cation exchange resin in synthesized wastewater. Chemosphere. 2004;56(2):141–7. https://doi.org/10.1016/j.chemosphere.2004.02.004 PMID: 15120560
9. Tan B. Removal of dyes and industrial dye wastes by magnesium chloride. Water Research. 2000;34(2):597–601. https://doi.org/10.1016/s0043-1354(99)00151-7
10. Akbal F, Camcı S. Copper, chromium and nickel removal from metal plating wastewater by electrocoagulation. Desalination. 2011;269(1–3):214–22. https://doi.org/10.1016/j.desal.2010.11.001
11. Heidmann I, Calmano W. Removal of Zn(II), Cu(II), Ni(II), Ag(I) and Cr(VI) present in aqueous solutions by aluminium electrocoagulation. J Hazard Mater. 2008;152(3):934–41. https://doi.org/10.1016/j.jhazmat.2007.07.068 PMID: 17854991
12. Peng H, Guo J, Li B, Liu Z, Tao C. High-efficient recovery of chromium (VI) with lead sulfate. Journal of the Taiwan Institute of Chemical Engineers. 2018;85:149–54. https://doi.org/10.1016/j.jtice.2018.01.028
13. Barakat MA. New trends in removing heavy metals from industrial wastewater. Arabian Journal of Chemistry. 2011;4(4):361–77. https://doi.org/10.1016/j.arabjc.2010.07.019
14. Pehlivan E, Cetin S. Sorption of Cr(VI) ions on two Lewatit-anion exchange resins and their quantitative determination using UV-visible spectrophotometer. J Hazard Mater. 2009;163(1):448–53. https://doi.org/10.1016/j.jhazmat.2008.06.115 PMID: 18692308
15. Bhaumik M, Setshedi K, Maity A, Onyango MS. Chromium(VI) removal from water using fixed bed column of polypyrrole/Fe3O4 nanocomposite. Separation and Purification Technology. 2013;110:11–9. https://doi.org/10.1016/j.seppur.2013.02.037
16. Michalak I, Chojnacka K, Witek-Krowiak A. State of the art for the biosorption process--a review. Appl Biochem Biotechnol. 2013;170(6):1389–416. https://doi.org/10.1007/s12010-013-0269-0 PMID: 23666641
17. Yang J, Yu M, Chen W. Adsorption of hexavalent chromium from aqueous solution by activated carbon prepared from longan seed: Kinetics, equilibrium and thermodynamics. Journal of Industrial and Engineering Chemistry. 2015;21:414–22. https://doi.org/10.1016/j.jiec.2014.02.054
18. Bansal M, Garg U, Singh D, Garg VK. Removal of Cr(VI) from aqueous solutions using pre-consumer processing agricultural waste: a case study of rice husk. J Hazard Mater. 2009;162(1):312–20. https://doi.org/10.1016/j.jhazmat.2008.05.037 PMID: 18573603
19. Omar A, Belhaj N, Elwafi W, Algmati N, Abozeed S. Removal of hexavalent chromium from aqueous solutions by olive pomace. In: Proceedings of the International Libyan Water Conference, 2018. https://www.researchgate.net/publication/360116285_Removal_of_Hexavalent_Chromium_from_Aqueous_Solutions_by_Olive_Pomace
20. Long W, Chen Z, Shi J, Yang S. Efficient Removal of Cr(VI) Ions in Petrochemical Wastewater Using Fe3O4@Saccharomyces cerevisiae Magnetic Nanocomposite. Nanomaterials (Basel). 2022;12(18):3250. https://doi.org/10.3390/nano12183250 PMID: 36145038

21. Blázquez G, Hernáinz F, Calero M, Martín-Lara MA, Tenorio G. The effect of pH on the biosorption of Cr (III) and Cr (VI) with olive stone. Chemical Engineering Journal. 2009;148(2–3):473–9. https://doi.org/10.1016/j.cej.2008.09.026
22. Kalyan Kumar M, Naik MM. Comparative studies of removal of hexavalent chromium Cr(VI) from wastewater using natural adsorbents prepared from neem leaves and sawdust. IJERT. 2015;4(09):IJERTV4IS090841. https://doi.org/10.17577/IJERTV4IS090841
23. Lee HV, Hamid SBA, Zain SK. Conversion of lignocellulosic biomass to nanocellulose: structure and chemical process. ScientificWorldJournal. 2014;2014:631013. https://doi.org/10.1155/2014/631013 PMID: 25247208
24. Basnet P, Ojha PK, Gyawali D, Ghimire KN, Paudyal H. Thermochemical study of Cr(VI) sequestration onto chemically modified Areca catechu and its recovery by desorptive precipitation method. Heliyon. 2022;8(8).
25. Lehmann J, Joseph S. Biochar for Environmental Management: An Introduction. Biochar for Environmental Management. Routledge. 2015. 1–13.
26. Lochan Aryal R, Thapa A, Raj Poudel B, Raj Pokhrel M, Dahal B, Paudyal H, et al. Effective biosorption of arsenic from water using La(III) loaded carboxyl functionalized watermelon rind. Arabian Journal of Chemistry. 2022;15(3):103674. https://doi.org/10.1016/j.arabjc.2021.103674
27. Boehm HP. Some aspects of the surface chemistry of carbon blacks and other carbons. Carbon. 1994;32(5):759–69.
28. Kadirvelu K, Thamaraiselvi K, Namasivayam C. Removal of heavy metals from industrial wastewaters by adsorption onto activated carbon prepared from an agricultural solid waste. Bioresour Technol. 2001;76(1):63–5. https://doi.org/10.1016/s0960-8524(00)00072-9 PMID: 11315812
29. Cha JS, Choi J-C, Ko JH, Park Y-K, Park SH, Jeong K-E, et al. The low-temperature SCR of NO over rice straw and sewage sludge derived char. Chemical Engineering Journal. 2010;156(2):321–7. https://doi.org/10.1016/j.cej.2009.10.027
30. Toles CA, Marshall WE, Wartelle LH, McAloon A. Steam- or carbon dioxide-activated carbons from almond shells: physical, chemical and adsorptive properties and estimated cost of production. Bioresource Technology. 2000;75(3):197–203. https://doi.org/10.1016/s0960-8524(00)00058-4
31. Kharrazi SM, Soleimani M, Jokar M, Richards T, Pettersson A, Mirghaffari N. Pretreatment of lignocellulosic waste as a precursor for synthesis of high porous activated carbon and its application for Pb (II) and Cr (VI) adsorption from aqueous solutions. Int J Biol Macromol. 2021;180:299–310. https://doi.org/10.1016/j.ijbiomac.2021.03.078 PMID: 33737183
32. Shrestha D. Efficiency of wood-dust of Dalbergia sisoo as low-cost adsorbent for rhodamine-b dye removal. Nanomaterials. 2021;11(9):2217.
33. Yunus ZM, Othman N, Al-Gheethi A, Hamdan R, Ruslan NN. Adsorption of heavy metals from mining effluents using honeydew peels activated carbon; isotherm, kinetic and column studies. Journal of Dispersion Science and Technology. 2020;42(5):715–29. https://doi.org/10.1080/01932691.2019.1709493
34. Huang G, Shi JX, Langrish TAG. Removal of Cr(VI) from aqueous solution using activated carbon modified with nitric acid. Chemical Engineering Journal. 2009;152(2–3):434–9. https://doi.org/10.1016/j.cej.2009.05.003
35. Rangabhashiyam S, Selvaraju N. Adsorptive remediation of hexavalent chromium from synthetic wastewater by a natural and ZnCl2 activated Sterculia guttata shell. Journal of Molecular Liquids. 2015;207:39–49. https://doi.org/10.1016/j.molliq.2015.03.018
36. Cha JS, Park SH, Jung S-C, Ryu C, Jeon J-K, Shin M-C, et al. Production and utilization of biochar: A review. Journal of Industrial and Engineering Chemistry. 2016;40:1–15. https://doi.org/10.1016/j.jiec.2016.06.002
37. Inoue K, Paudyal H, Nakagawa H, Kawakita H, Ohto K. Selective adsorption of chromium(VI) from zinc(II) and other metal ions using persimmon waste gel. Hydrometallurgy. 2010;104(2):123–8. https://doi.org/10.1016/j.hydromet.2010.05.005
38. Xu Y, Zhang J, Qian G, Ren Z, Xu ZP, Wu Y. Effective Cr(VI) removal from simulated groundwater through the hydrotalcite-derived adsorbent. Ind Eng Chem Res. 2010;49(6):2752–8. https://doi.org/10.1021/ie901469c
39. Malkoc E, Nuhoglu Y, Abali Y. Cr(VI) adsorption by waste acorn of Quercus ithaburensis in fixed beds: Prediction of breakthrough curves. Chemical Engineering Journal. 2006;119(1):61–8. https://doi.org/10.1016/j.cej.2006.01.019
40. Chen S, Yue Q, Gao B, Li Q, Xu X, Fu K. Adsorption of hexavalent chromium from aqueous solution by modified corn stalk: a fixed-bed column study. Bioresour Technol. 2012;113:114–20. https://doi.org/10.1016/j.biortech.2011.11.110 PMID: 22189077
41. Mitra T, Bar N, Das SK. Rice husk: green adsorbent for Pb(II) and Cr(VI) removal from aqueous solution—column study and GA–NN modeling. SN Appl Sci. 2019;1(5). https://doi.org/10.1007/s42452-019-0513-5
42. Wang W, Li M, Zeng Q. Adsorption of chromium(VI) by strong alkaline anion exchange fiber in a fixed-bed column: Experiments and models fitting and evaluating. Separation Purif Technol. 2015;149:16–23.
43. Malkoc E, Nuhoglu Y. Fixed bed studies for the sorption of chromium(VI) onto tea factory waste. Chemical Engineering Science. 2006;61(13):4363–72. https://doi.org/10.1016/j.ces.2006.02.005
44. Fseha YH, Eniola JO, Sizirici B, Stephen S, Yildiz I, Khaleel A. Application of natural earth-based materials as adsorbents for the treatment of chromium(VI)-contaminated tannery wastewater: Box-Behnken and fixed-bed column optimization. Sustainable Chemistry for the Environment. 2024;7:100127.
45. Cruz-Olivares J, Pérez-Alonso C, Martínez-Barrera G, Roa-Morales G, López-Téllez G, Martín del Campo-López E. Modeling and scaling up of the Cr(VI) adsorption process by using Mexicalcite natural mineral in a packed bed column. Results in Engineering. 2022;16:100687.
46. Sarkar S, Bar N, Das SK. Cr(VI) and Cu(II) removal from aqueous solution in fixed bed column using rice bran; experimental, statistical and GA modelling. Journal of the Indian Chemical Society. 2021;98(11):100216. https://doi.org/10.1016/j.jics.2021.100216
47. Fauzia S, Aziz H, Dahlan D, Zein R. Modeling for removal of Cr(VI) and Pb(II) using sago bark (Metroxylon sagu) by fixed-bed column method. Egypt J Chem. 2021.

48. Yahya MD, Abubakar H, Obayomi KS, Iyaka YA, Suleiman B. Simultaneous and continuous biosorption of Cr and Cu(II) ions from industrial tannery effluent using almond shell in a fixed bed column. Results Eng. 2020;6:100113.
49. Maheshwari U, Gupta S. Removal of Cr(VI) from wastewater using activated neem bark in a fixed-bed column: interference of other ions and kinetic modeling studies. Desalination and Water Treatment. 2016;57(18):8514–25. https://doi.org/10.1080/19443994.2015.1030709
50. Yakout SM, Hassan MR, Omar HA. Fixed-bed column study for the removal of hexavalent chromium ions from aqueous solutions via pyrolysis of rice husk. Desalination and Water Treatment. 2019;170:128–37.
51. Rangabhashiyam S, Nandagopal MSG, Nakkeeran E, Selvaraju N. Adsorption of hexavalent chromium from synthetic and electroplating effluent on chemically modified Swietenia mahagoni shell in a packed bed column. Environ Monit Assess. 2016;188(7):411. https://doi.org/10.1007/s10661-016-5415-z PMID: 27312254
52. Pandey PK, Sharma SK. Removal of Cr(VI) and Pb(II) from Wastewater by ZeoliteNaX in Fixed Bed Column. Water Conserv Sci Eng. 2017;2(3):61–5. https://doi.org/10.1007/s41101-017-0026-2
53. Mohanta S, Sahu MK, Mishra PC, Giri AK. Removal of Cr (VI) from aqueous solution by activated charcoal derived from Sapindus trifoliate L fruit biomass using continuous fixed bed column studies. Water Sci Technol. 2021;84(1):55–65. https://doi.org/10.2166/wst.2021.217 PMID: 34280154
54. Novera TM, Tabassum M, Bardhan M, Islam MdA, Islam MdA. Chemical modification of betel nut husk prepared by sodium hydroxide for methylene blue adsorption. Applied Water Science. 2021;11(4):66. https://doi.org/10.1007/s13201-021-01394-5
55. Cundari L, Sari KF, Anggraini L. Characteristic of betel nuts activated carbon and its application to Jumputan wastewater treatment. IOP Conf Ser: Mater Sci Eng. 2018;345:012041. https://doi.org/10.1088/1757-899x/345/1/012041
56. Narmatha M. Biosorption of basic yellow dye using leaf sheath powder of Areca catechu (betel nut tree). Research Journal of Chemical Sciences. 2022;12(2):1–9.
57. Herlinawati H, Sihombing L, Kembaren A, Simatupang L, Adhani R. Analysis of Fe metal adsorption in industrial wastewater using adsorbents from betel nut skin. JPendidikKim. 2023;15(1):35–40.
58. Rahman MA, Hasan MA, Salam MA, Salam A, Siddique NEA, Alam AS. Betel-nut peel as an adsorbent in the removal of Cd, Cr and Pb from aqueous solutions. Pakistan Journal of Analytical & Environmental Chemistry. 2012;13(2):51.
59. Kulkarni K, Sudheer V, R Girish C. Phenol adsorption from wastewater using cashew nut shells as adsorbent. IJET. 2018;7(3):966. https://doi.org/10.14419/ijet.v7i3.9771
60. Jothibasu S, Mohanamurugan S, Vijay R, Lenin Singaravelu D, Vinod A, Sanjay M. Investigation on the mechanical behavior of areca sheath fibers/jute fibers/glass fabrics reinforced hybrid composite for light weight applications. Journal of Industrial Textiles. 2018;49(8):1036–60. https://doi.org/10.1177/1528083718804207
61. Shrestha D. Applications of functionalized porous carbon from bio-waste of Alnus nepalensis in energy storage devices and industrial wastewater treatment. Heliyon. 2023;9(11):e21804.
62. Basnet P, Gyawali D, Ghimire KN, Paudyal H. Phosphoric acid activated Areca catechu as an efficient biosorbent for Cr(VI) sequestration from simulated and industrial effluent. Separation Science and Technology. 2025;60(6):561–82. https://doi.org/10.1080/01496395.2025.2451912
63. Vijayaraghavan K, Jegan J, Palanivelu K, Velan M. Batch and column removal of copper from aqueous solution using a brown marine alga Turbinaria ornata. Chemical Engineering Journal. 2005;106(2):177–84. https://doi.org/10.1016/j.cej.2004.12.039
64. Homagai PL, Poudel R, Paudyal H, Ghimire KN, Bhattarai A. Adsorption of nitrate and nitrite anion by modified maize stalks from aqueous solutions. Environmental Science and Pollution Research. 2023;30(19):54682–93. https://doi.org/10.1007/s11356-023-26179-y
65. Paudyal H, Pangeni B, Inoue K, Kawakita H, Ohto K, Alam S. Adsorptive removal of fluoride from aqueous medium using a fixed bed column packed with Zr(IV) loaded dried orange juice residue. Bioresour Technol. 2013;146:713–20. https://doi.org/10.1016/j.biortech.2013.07.014 PMID: 23916190
66. Demiral H, Demiral İ, Tümsek F, Karabacakoğlu B. Adsorption of chromium(VI) from aqueous solution by activated carbon derived from olive bagasse and applicability of different adsorption models. Chemical Engineering Journal. 2008;144(2):188–96. https://doi.org/10.1016/j.cej.2008.01.020
67. Beer. Bestimmung der Absorption des Rothen Lichts in Farbigen Flüssigkeiten. Annalen der Physik. 1852;162(5):78–88. https://doi.org/10.1002/andp.18521620505
68. Kavianinia I, Plieger PG, Kandile NG, Harding DRK. Fixed-bed column studies on a modified chitosan hydrogel for detoxification of aqueous solutions from copper (II). Carbohydr Polym. 2012;90(2):875–86. https://doi.org/10.1016/j.carbpol.2012.06.014 PMID: 22840015
69. Pellenz L, de Oliveira CRS, da Silva Júnior AH, da Silva LJS, da Silva L, Ulson de Souza AA. A comprehensive guide for characterization of adsorbent materials. Separation and Purification Technology. 2023;305:122435.
70. Skic K, Adamczuk A, Gryta A, Boguta P, Tóth T, Jozefaciuk G. Surface Areas and Adsorption Energies of Biochars Estimated from Nitrogen and Water Vapor Adsorption Isotherms. Sci Rep. 2024;14(1):30362.
71. le guillou C, Rouzaud J, Bonal L, Quirico E, Derenne S, Remusat L. High resolution TEM of chondritic carbonaceous matter: Metamorphic evolution and heterogeneity. Meteorit & Planetary Scien. 2012;47(3):345–62. https://doi.org/10.1111/j.1945-5100.2012.01336.x
72. Khalfaoui M, Knani S, Hachicha MA, Lamine AB. New theoretical expressions for the five adsorption type isotherms classified by BET based on statistical physics treatment. J Colloid Interface Sci. 2003;263(2):350–6. https://doi.org/10.1016/s0021-9797(03)00139-5 PMID: 12909023

73. Kumar P, Prajapati KB, Mahajan AK, Pant D, Meena NK, Kumar A, et al. Evaluating feasibility of biosorption technique for heavy metals removal: limitations and future perspective. International Journal of Environmental Analytical Chemistry. 2022;104(18):6401–25. https://doi.org/10.1080/03067319.2022.2145196
74. Mona S, Kaushik A, Kaushik CP. Biosorption of chromium(VI) by spent cyanobacterial biomass from a hydrogen fermentor using Box-Behnken model. International Biodeterioration & Biodegradation. 2011;65(4):656–63. https://doi.org/10.1016/j.ibiod.2011.04.002
75. Rai R, Aryal RL, Paudyal H, Gautam SK, Ghimire KN, Pokhrel MR. Acid-Treated Pomegranate Peel: an Efficient Biosorbent for the Excision of Hexavalent Chromium from Wastewater. Heliyon. 2023;9(5).
76. Nano I. FTIR functional group database table with search. https://instanano.com/all/characterization/ftir/ftir-functional-group-search/ 2021.
77. Pant BD, Neupane D, Paudel DR, Chandra Lohani P, Gautam SK, Pokhrel MR. Efficient biosorption of hexavalent chromium from water by modified arecanut leaf sheath. Heliyon. 2022;8(4):e09283.
78. Rangabhashiyam S, Suganya E, Selvaraju N. Packed bed column investigation on hexavalent chromium adsorption using activated carbon prepared from Swietenia mahogani fruit shells. Desalination and Water Treatment. 2016;57(28):13048–55. https://doi.org/10.1080/19443994.2015.1055519
79. Ahmadi M, Kouhgardi E, Ramavandi B. Physico-chemical study of dew melon peel biochar for chromium attenuation from simulated and actual wastewaters. Korean J Chem Eng. 2016;33(9):2589–601. https://doi.org/10.1007/s11814-016-0135-1
80. Han R, Wang Y, Zhao X, Wang Y, Xie F, Cheng J, et al. Adsorption of methylene blue by phoenix tree leaf powder in a fixed-bed column: experiments and prediction of breakthrough curves. Desalination. 2009;245(1–3):284–97. https://doi.org/10.1016/j.desal.2008.07.013
81. Han R, Zhang J, Zou W, Xiao H, Shi J, Liu H. Biosorption of copper(II) and lead(II) from aqueous solution by chaff in a fixed-bed column. J Hazard Mater. 2006;133(1–3):262–8. https://doi.org/10.1016/j.jhazmat.2005.10.019 PMID: 16298055
82. Thrikkykkal H, Antu R, P S H. Remediation of Pb (II), Cd (II), and Zn (II) from aqueous solutions using porous (styrene-divinylbenzene)/Cu-Ni bimetallic nanocomposite microspheres: continuous fixed-bed column study. Water Sci Technol. 2023;87(9):2277–91. https://doi.org/10.2166/wst.2023.101 PMID: 37186630
83. Baral SS, Das N, Ramulu TS, Sahoo SK, Das SN, Chaudhury GR. Removal of Cr(VI) by thermally activated weed Salvinia cucullata in a fixed-bed column. J Hazard Mater. 2009;161(2–3):1427–35. https://doi.org/10.1016/j.jhazmat.2008.04.127 PMID: 18571842
84. Jain M, Garg VK, Kadirvelu K. Cadmium(II) sorption and desorption in a fixed bed column using sunflower waste carbon calcium-alginate beads. Bioresour Technol. 2013;129:242–8. https://doi.org/10.1016/j.biortech.2012.11.036 PMID: 23247153
85. Singh A, Kumar D, Gaur JP. Continuous metal removal from solution and industrial effluents using Spirogyra biomass-packed column reactor. Water Res. 2012;46(3):779–88. https://doi.org/10.1016/j.watres.2011.11.050 PMID: 22169159
86. González M, Laureano-Anzaldo C, Perez Fonseca A, Arellano M, Robledo-Ortíz J. A discussion on linear and non-linear forms of Thomas equation for fixed-bed adsorption column modeling. Revista Mexicana de Ingeniería Química. 2021;20:875–84. https://doi.org/10.24275/rmiq/Fen2337
87. Reynolds TD, Richards PA. Unit Operations and Processes in Environmental Engineering. PWS Publishing Company. 1996.
88. Bulgariu D, Bulgariu L. Sorption of Pb(II) onto a mixture of algae waste biomass and anion exchanger resin in a packed-bed column. Bioresour Technol. 2013;129:374–80. https://doi.org/10.1016/j.biortech.2012.10.142 PMID: 23262014
89. Omitola OB, Abonyi MN, Akpomie KG, Dawodu FA. Adams-Bohart, Yoon-Nelson, and Thomas modeling of the fixed-bed continuous column adsorption of amoxicillin onto silver nanoparticle-maize leaf composite. Applied Water Science. 2022;12(5):94. https://doi.org/10.1007/s13201-022-01624-4
90. Chowdhury ZZ, Zain SM, Rashid AK, Rafique RF, Khalid K. Breakthrough Curve Analysis for Column Dynamics Sorption of Mn(II) Ions from Wastewater by Using Mangostana garcinia Peel-Based Granular-Activated Carbon. Journal of Chemistry. 2012;2013(1). https://doi.org/10.1155/2013/959761
91. Zhong Q-Q, Yue Q-Y, Li Q, Gao B-Y, Xu X. Removal of Cu(II) and Cr(VI) from wastewater by an amphoteric sorbent based on cellulose-rich biomass. Carbohydr Polym. 2014;111:788–96. https://doi.org/10.1016/j.carbpol.2014.05.043 PMID: 25037417
92. Aksu Z, Gönen F. Biosorption of phenol by immobilized activated sludge in a continuous packed bed: prediction of breakthrough curves. Process Biochemistry. 2004;39(5):599–613. https://doi.org/10.1016/s0032-9592(03)00132-8
93. Ahmad AA, Hameed BH. Fixed-bed adsorption of reactive azo dye onto granular activated carbon prepared from waste. J Hazard Mater. 2010;175(1–3):298–303. https://doi.org/10.1016/j.jhazmat.2009.10.003 PMID: 19883979
94. Yoon YH, Nelson JH. Application of gas adsorption kinetics. I. A theoretical model for respirator cartridge service life. Am Ind Hyg Assoc J. 1984;45(8):509–16. https://doi.org/10.1080/15298668491400197 PMID: 6475758
95. da Costa TB, da Silva TL, Costa CSD, da Silva MGC, Vieira MGA. Chromium adsorption using Sargassum filipendula algae waste from alginate extraction: Batch and fixed-bed column studies. Chemical Engineering Journal Advances. 2022;11:100341. https://doi.org/10.1016/j.ceja.2022.100341
96. Wagih N, Mahmoud MM, Elbaz AA, EL-Moniry D. Oil removal using agricultural wastes adsorbents in a fixed bed column as a pretreatment in RO systems. Desalination and Water Treatment. 2024;320:100811.
97. Bohart GS, Adams EQ. Some aspects of the behavior of charcoal with respect to chlorine 1. J Am Chem Soc. 1920;42(3):523–44. https://doi.org/10.1021/ja01448a018

98. Gutiérrez-Segura E, Colín-Cruz A, Solache-Ríos M, Fall C. Removal of Denim Blue from Aqueous Solutions by Inorganic Adsorbents in a Fixed-Bed Column. Water Air Soil Pollut. 2012;223(8):5505–13. https://doi.org/10.1007/s11270-012-1299-x

99. Jung K, Jeong T, Choi BH, Jeong Kang H, Ahn K. Phosphate adsorption from aqueous solution by Laminaria japonica-derived biochar-calcium alginate beads in a fixed-bed column: Experiments and prediction of breakthrough curves. Env Prog and Sustain Energy. 2017;36(5):1365–73. https://doi.org/10.1002/ep.12580

100. Bensadek S, Aguedal H, Iddou A, Aziz A. Biosorption of Chromium(VI) in a Fixed-Bed Column using Adsorbent Biomass. Key Engineering Materials. 2019;800:157–63.

101. Banerjee M, Bar N, Basu RK, Das SK. Comparative study of adsorptive removal of Cr(VI) ion from aqueous solution in fixed bed column by peanut shell and almond shell using empirical models and ANN. Environ Sci Pollut Res Int. 2017;24(11):10604–20. https://doi.org/10.1007/s11356-017-8582-8 PMID: 28283971

102. Ahamad KU, Jawed M. Breakthrough studies with mono- and binary-metal ion systems comprising of Fe(II) and As(III) using community prepared wooden charcoal packed columns. Desalination. 2012;285:345–51.

103. Li W, Yue Q, Tu P, Ma Z, Gao B, Li J, et al. Adsorption characteristics of dyes in columns of activated carbon prepared from paper mill sewage sludge. Chemical Engineering Journal. 2011;178:197–203. https://doi.org/10.1016/j.cej.2011.10.049

104. Mohammad YS, Shaibu-Imodagbe E, Igboro Sunday B, Giwa A, Okuofu A. Adsorption of phenol from refinery wastewater using rice husk activated carbon. Iranica Journal of Energy and Environment. 2014;5(4):393–9. https://doi.org/10.5829/idosi.ijee.2014.05.04.07

105. Mitra T, Das SK. Cr(VI) removal from aqueous solution using Psidium guajava leaves as green adsorbent: column studies. Appl Water Sci. 2019;9(7):153. https://doi.org/10.1007/s13201-019-1029-2